1 **B cell heterogeneity in human tuberculosis highlights compartment-specific phenotype and**

2 **functional roles**

3 **Robert Krause[1,2], Paul Ogongo[1,2,3], Liku Tezera[4,5,6], Mohammed Ahmed[1,2], Ian Mbano[1,2], Mark**

4 **Chambers[1,2], Abigail Ngoepe[1], Magalli Magnoumba[1,2], Daniel Muema[1,2], Farina Karim[1,2], Khadija**

5 **Khan[1,2], Kapongo Lumamba[1], Kievershen Nargan[1], Rajhmun Madansein[7], Adrie Steyn[1,2,8,9], Alex K**

6 **Shalek[10], Paul Elkington[4,5], Al Leslie[1,2,6,*]**

7 1 Africa Health Research Institute, Durban, South Africa.

8 2 School of Laboratory Medicine and Medical Sciences, University of KwaZulu-Natal, Durban, South

9 Africa.

10 3 Institute of Primate Research, National Museums of Kenya, Nairobi, Kenya.

11 4 National Institute for Health Research Southampton Biomedical Research Centre, School of Clinical

12 and Experimental Sciences, Faculty of Medicine, and

13 5 Institute for Life Sciences, University of Southampton, Southampton, United Kingdom.

14 6 Division of Infection and Immunity, University College London, London, United Kingdom.

15 7 Department of Cardiothoracic Surgery, Nelson Mandela School of Medicine, University of KwaZulu-

16 Natal, Durban, South Africa.

17 8 Department of Microbiology and

18 9 Center for AIDS Research and Center for Free Radical Biology, University of Alabama at Birmingham,

19 Birmingham, Alabama, USA.

20 10 Institute for Medical Engineering & Science, Department of Chemistry, Koch Institute for

21 Integrative Cancer Research, Massachusetts Institute of Technology, Cambridge, MA 02139, USA;

22 Ragon Institute of MGH, MIT, and Harvard, Cambridge, MA 02139, USA; Broad Institute of MIT and

23 Harvard, Cambridge, MA 02142, USA

24   * Corresponding author: Alasdair Leslie email at al.leslie@ahri.org

25

Abstract

B cells are important in tuberculosis (TB) immunity, but their role in the human lung is understudied. Here, we characterize B cells from lung tissue and matched blood of TB patients and found they are decreased in the blood and increased in the lungs, consistent with recruitment to infected tissue, where they are located in granuloma associated lymphoid tissue (GrALT). Flow cytometry and transcriptomics identified multiple B cell populations in the lung, including those associated with tissue resident memory, germinal centers, antibody secretion, proinflammatory atypical B cells, and regulatory B cells, some of which are expanded in TB disease. Additionally, TB lungs contained high levels of *Mtb*-reactive antibodies, specifically IgM, which promoted *Mtb* phagocytosis. Overall, these data reveal the presence of functionally diverse B cell subsets in TB diseased lung and suggest several potential localized roles that may represent a target for interventions to promote immunity or mitigate immunopathology.

38

39

40

41

42

43

44

45

Introduction

In 2021, *Mycobacterium tuberculosis* (*Mtb*) was estimated to infect a quarter of the world's population, cause tuberculosis (TB) in 10.6 million and kill 1.6 million people [1]. *Mtb* is spread when exhaled/coughed aerosolized droplets are inhaled into another individual's lungs where infection propagates. A characteristic of pulmonary TB is the generation of granuloma [2], typically formed from clusters of infected alveolar macrophages surrounded by a cuff of lymphocytes, including T cells, B cells and various innate lymphoid cells. In addition, B cells are frequently observed within lymphocyte aggregates near granuloma, referred to as granuloma-associated lymphoid tissue (GrALT) [3]. GrALT has been observed in mice [4-8], non-human primates (NHP) [8-10] and humans [8,11,12] and is typically associated with protective immunity. However, the role of B cells in the immune response to TB within the lung remains poorly understood.

In humans, TB leads to a reduction in circulating B cells [11,13-17], which recover following successful treatment [11,15,18]. In mice, B cell knock out or depletion results in greater susceptibility to TB [4,6], with adoptive transfer resulting in reversed lung pathology [7,19]. In non-human primates, B cell depletion increases bacterial burden in lung lesions [10]. Mechanistically, recent studies implicate B cells in orchestrating the CD4$^+$ T cell response within GrALT, affecting both the T_H1 and T_H17 protective responses [3,20-23]. In addition, B cell follicle area correlated with lung *IL17* mRNA levels, and B cells from pleural fluid were critical mediators of the IL17 and IL22 responses [24-26]. Tissue resident memory B cells reside in the lung and can mature into antibody secreting plasma cells [27]. Several studies demonstrate a role for *Mtb* specific antibodies in protective immunity to TB in both NHPs and humans [22,23,28-32]. Furthermore, active and latent TB can be differentiated based on antibody glycosylation profiles [29,33] and the resulting differences in the Fc effector functions (binding FcγRIII) including antibody mediated phagocytosis [29].

Together, these studies demonstrate B cell involvement during TB and highlight important canonical and non-canonical functions that contribute to TB immunity. However, data from humans in the lung

3

71   compartment is lacking. Here, we demonstrate that TB infected lung tissues are enriched for CD19^{+} B

72   cells, which are associated with granuloma. Lung B cells were predominantly of a memory phenotype

73   and expressed markers associated with residency and germinal center homing. In addition, the lung

74   was enriched for antibody secreting cells (ASC) and unique putative regulatory B cell phenotypes.

75   Using a granuloma biomimetic model, we found that B cells from healthy donors contribute to control

76   of *Mtb* growth, whilst this function is inconsistent in TB patients, suggesting potential impairment of

77   these cells during active disease. Finally, TB diseased lung tissue was enriched for *Mtb* specific

78   antibodies relative to control lungs, especially IgM, which enhanced *Mtb* phagocytosis by primary

79   human cells. These findings highlight the diversity of B cell function in human TB.

80

81   **Results**

82   **Comparison of CD19^{+} B cells in blood and lung tissue compartments**

83   First, we compared the relative frequencies of B cells in the peripheral blood of non-TB controls, latent

84   TB (LTBI) and active TB (ATBI) patients (**Fig. 1A and B**). LTBI was confirmed by a positive Interferon

85   Gamma Release Assay (IGRA) test in participants with no signs, symptoms, or history of TB disease.

86   Non-TB controls were similarly asymptomatic but were IGRA negative [16]. The Frequency of CD19^{+} B

87   cells was reduced in the blood of LTBI and ATBI compared to healthy controls, consistent with

88   published data [11,13-16]. We then measured the frequency of B cells in homogenized TB-diseased lung

89   tissue, obtained from individuals enrolled in the AHRI lung resection cohort [34], undergoing surgical

90   resection to treat TB sequelae (**Fig. 1A and C**). Additional samples were analysed from patients with

91   no history of TB, who were undergoing surgical resection of lung cancer and from whom

92   macroscopically uninvolved tissue was obtained. These controls were not IGRA tested, and thus latent

93   TB infection could not be excluded, although TB prevalence is so high in KwaZulu-Natal, most donors

94   are highly likely to have been TB-exposed. TB diseased lung tissue was highly enriched for B cells

95   compared to matched blood samples, with a median frequency of approximately 9% of CD45^{+},

96 reaching as high as 31% in some patients (**Fig. 1C**), significantly higher than in lung tissue from non-TB

97 controls (median of 3%). In contrast, CD3^{+} T cells were not significantly enriched in TB diseased lung

98 tissue compared to matched blood, although these cells were more abundant than B cells (median

99 72%, **Fig. 1D**).

100 **Histological localization of B cells in proximity to granulomatous structures**

101 To determine the localization of B cells within TB diseased lung tissue, we conducted histological

102 assessment of lung sections from participants with distinct granulomatous lesions. The canonical TB

103 lung granuloma has a CD68^{+} macrophage core surrounded by a cuff of CD45^{+} lymphocytes (**Fig. 2A**).

104 This cuff comprises CD3^{+} T cells with some also present within the granuloma core. CD20^{+} staining

105 reveals a distinct B cell aggregate in close association with the granuloma, consistent with previously

106 described GrALT [8,11,12]. B cells also associate with the granuloma cuff, primarily adjacent to the GrALT.

107 The GrALT also contains CD3^{+} T cells, consistent with previous reports and with lymphoid follicles. In

108 addition, CD21 staining is present within the centre of the GrALT, suggestive of follicular dendritic cells

109 [8,35], although mature B cells can express CD21 within germinal centres [36]. Of interest were the staining

110 patterns of anti-CD20, anti-CD3 and anti-CD21 in particular (**Supplementary Figure 1**). CD20 and CD3

111 staining are characteristic of lymphoid cells whereas CD21 stained cells displaying a more dendrite-

112 like pattern. The CD20^{+} cells occupy most of the aggregate, whereas the CD3^{+} cells are more

113 peripheral, and the CD21^{+} cells seem to occupy the centre of the aggregate. Quantitation of

114 granulomatous lesion containing lungs from 5 different TB patients show a roughly equivalent

115 frequency of T and B cells associated with lung granuloma, in the region of 20% of nucleated

116 (haematoxylin+) cells (**Fig. 2B**). As some surface markers are co-expressed by different cells, the total

117 exceeds 100%. Overall, these data suggest that B cells are enriched in the lung during TB infection in

118 humans and make up a significant proportion of granuloma-associated lymphocytes.

119

Prominent memory and antibody secreting cell (ASC) phenotypes in the lung compartment including

CD69$^+$ memory

Next, we examined the phenotype of B cells in matched blood and lung samples from TB diseased participants and non-TB controls (**Fig. 3**). First, we examined the B cell maturation state based on the canonical memory marker CD27 and activation marker CD38 [37](**Fig. 3A**). Notably, CD27$^+$CD38$^-$ memory B cells were enriched in TB diseased lung tissue compared to matched blood, which was dominated by CD27$^-$CD38$^-$ naïve and CD27$^-$CD38$^+$ transitional B cells (**Fig. 3B**). The same trend was observed in control lung samples, although the enrichment of memory B cells was not significant and memory B cells were significantly more abundant in TB diseased compared to control lungs. CD27$^+$CD38^{hi} antibody secreting cells (ASCs) were present in lung tissue, and were significantly enriched compared to matched blood, but were significantly higher in non-TB diseased lung tissue. In addition, lung derived memory B cells were highly enriched for the expression of the tissue residence marker CD69 [27](**Fig. 3C**). Finally, from a subset of lung samples, lung draining lymph nodes were studied as an alternative comparator tissue enriched with B cells (**Fig. 3D, Supplementary Fig. 2**)[38]. Lung tissue had increased memory subsets compared to matched lymph nodes, and as expected, lymph nodes contained a low prevalence of ASCs [38].

Transcriptional analysis of lung derived B cells

Having observed an enrichment of memory B cell subsets in TB diseased lung tissue, we interrogated these in a single cell RNA sequence (scRNAseq) analysis of additional lung tissue samples obtained from the same lung cohort. Of a total 20962 single cells recovered from 9 resected TB patient lungs, 404 displayed canonical B cell markers including the lineage markers CD19 and CD20. We focused on leukocytes, although scRNAseq analysis demonstrated the presence of other stromal cells in the lung homogenates such as epithelial cells and fibroblasts (manuscript in preparation). Sub clustering of this limited dataset nevertheless identified a total of 7 unique B cell subsets, shown by UMAP projection (**Fig. 4A**). A curated list of B cell genes was used to assign putative functional phenotypes to the 7

145   subsets (**Fig. 4B**). This includes populations expressing genes associated with memory B cells (3 and 4)

146   which expressed CD21, a B cell coreceptor involved in T cell dependent signalling, in addition to CD27

147   and CD38, and ASCs (5 and 6), expressing the highest levels of genes associated with immunoglobulin

148   heavy chains, including subclasses IgG 1-4 as well as IgA. These cells also expressed CD138 and BLIMP1,

149   both markers of long-lived plasma cells [37,39], and IgJ and PPIB, involved in the production of IgM and

150   IgA antibodies [39-42] and protein secretion respectively [43]. Consistent with flow cytometry data, lung B

151   cells express the gene encoding CD69, especially subsets 1 and 2, which also express CCR7 and CXCR4.

152   Subsets 3 and 4 lack CCR7 but co-express CXCR4 and CXCR5. All three chemokine receptors are

153   involved in trafficking within the germinal centre (GC) [7,39,44], and may thus represent B cell populations

154   associated with GrALT. In line with this, populations 3 and 4 express Bcl6, a key regulator of the GC

155   response [45-47] and AICDA, which is expressed during B cell receptor (BCR) affinity maturation [48], as well

156   as the GC marker CD10[35]. Population 3 and 4 also express the highest levels of CD21 and CD22, both

157   essential to B cell GC survival [36,49] and CD79a, a marker of mature B cells [9]. The immunoglobulin and

158   CD79a transcript abundance generally increased from populations 0 to 6, and since both are

159   associated with the B cell surface receptor, this also suggests the local B cell population is maturing[9,50].

160   Several genes associated with genome replication (MCM4) [45], proliferation (MKi67) [42,45] and cell cycle

161   progression (MYBL2) [46] are also highly expressed. Population 0, on the other hand, is distinguished by

162   CD11c expression, which is a marker of atypical B cells [51-54], and ZEB2, recently identified as a key

163   transcription factor promoting the development of this cell type [55]. This population also expresses

164   genes encoding TLR2, TLR4 and MyD88, a common adaptor molecule for all TLRs except TLR3 [56].

165   Interestingly, BANK-1 was recently shown to signal together with MyD88 and TLRs to co-ordinate

166   innate immune signalling B cells, including the production of IL-8, and population 0 expresses both

167   BANK-1 and high levels of the IL-8 gene [57]. Thus, scRNAseq data supports the presence of GC-like B cell

168   populations, ASC-like and atypical/innate-like B cells in TB diseased lung tissue. The next aim was to

169   identify similarities between these B cell populations putatively identified by sequencing, with those

170   identified by flow cytometry.

171 **Transcriptional heterogeneity of B cells translates to several B cell phenotypes identified by flow**

172 **cytometry, highlighting compartmental heterogeneity**

173   We obtained 13 additional lung samples and analysed lung homogenate and matched blood samples

174   by flow cytometry using three separate antibody panels, each elaborating on a core set of shared

175   markers included in **Fig. 1** and **3**: CD19, CD27, CD38, IgD and IgM (**Fig. 5**). We initially analysed these

176   data using an unbiased clustering algorithm to identify unique B cell populations based on the markers

177   in each flow cytometry panel (**Fig. 5A-C**). Consistent with the initial flow cytometry profiling (**Fig. 3**),

178   the main phenotypic differences were based on B cell maturation, with the blood containing more

179   transitional and naïve B cells, compared to increased memory and ASC frequencies in the lung. A single

180   patient sample was used to generate a representative tSNE plot (**Fig. 5)**, to gain an overview of the

181   number of unique B cell phenotypes associated with the lung and blood compartments. We then

182   interrogated any phenotypes of interest in a total of 13 TB diseased patients to assess compartmental

183   differences (**Fig. 6, Supplementary Fig. 3**).

184   Common to all three panels was a prominent B cell phenotype that was $CD27^{mid/lo}$, $CD38^{-}$, IgD^{-} and

185 IgM^{-} (**Fig. 5A** green**, B** blue**, C** tan) designated as an atypical/double negative (DN) memory population.

186   The double negative phenotype is defined as being negative for CD27 and IgD [51]. This was expanded

187   in the lung compared to matched blood. As shown in flow panel 1 (**Fig. 5A**), two such populations were

188   apparent, both of which express the key atypical B cell marker CD11c, consistent with the scRNAseq

189   data (**Fig. 4**). The second population resembles an activated double negative (DN2) phenotype, as it

190   expresses the highest levels of CD11c, and is $CD20^{hi}$ and $CXCR5^{-}$ [51-54]. This activated DN2 phenotype

191   was enriched in the lung when assessed across the 13 patients (**Fig. 6A, Supplementary Fig. 3A**).

192   Several studies have observed an enrichment of DN2 B cells in the blood under inflammatory

193   conditions [51-54] and further enrichment in TB diseased lung supports their potential importance at the

194   site of infection. Additionally, in the second panel, the putative atypical B cell population (**Fig. 5B** blue)

195 expresses high levels of CXCR3, which would facilitate homing to inflamed tissue sites via CXCL10

196 [27,39,58].

197 Naïve (**Fig. 5**, red) and transitional (**Fig. 5**, orange) B cell phenotypes were dominant in the blood, as

198 seen in the initial flow cytometry phenotyping data (**Fig. 3**), with the transitional phenotype expressing

199 CD10 and CD138 as expected (**Fig. 5A**)[37]. Both naïve and transitional phenotypes displayed high

200 expression of CXCR5 associated with homing to germinal centres (**Fig. 5B, Fig. 6B, Supplementary Fig.**

201 **3B**) [7,39,44], and both phenotypes were enriched in circulation (**Fig. 6B**). The naïve GC centroblast-like

202 phenotype (**Fig. 5B**, lime green) expressed homing markers including CD62L, CXCR4, CXCR5 and CCR7,

203 consistent with population 1 and 2 identified by scRNAseq (**Fig. 4**). A transitional B cell phenotype,

204 $CD24^+CD38^+$, which is associated with regulatory functions [42,59], was enriched in the blood compared

205 to lung (**Fig. 5C, Fig. 6C, Supplementary Fig. 3C**). In contrast, the purple population in **Fig. 5B**, which

206 expressed a phenotype resembling the putative GC populations 3 and 4 from the scRNAseq data (**Fig.**

207 **4**), being $CD27^+CXCR5^+CD62L^-CD69^+CCR7^+$ and $CCR6^+$, was significantly enriched in the lung (**Fig. 6D,**

208 **Supplementary Fig. 3D**).

209 The $CD27^+CD38^{hi}$ ASC-like populations observed by scRNAseq (**Fig. 4**) were also apparent by flow

210 cytometry in the lung, including $CD138^+$ plasma cells (**Fig. 5A**). ASCs could be separated based on

211 expression of CXCR3 and CD62L (**Fig. 5B**). CXCR3 facilitates homing to sites of inflammation, and CD62L

212 (L-selectin) is essential for migration of lymphocytes into tissue and is lost as B cells mature into

213 plasmablasts and finally plasma cells [60]. $CXCR3^+CD62L^+$ ASC were significantly enriched in the blood,

214 whereas $CXCR3^+CD62L^-$ ASC were enriched in the lung (**Fig. 5B, Fig. 6E and Supplementary Fig. 3E**),

215 consistent with antibody secreting populations (5 and 6) observed by sequencing (**Fig. 4**). In addition,

216 two phenotypes associated with regulatory functions were significantly associated with the lung

217 environment, one expressing a $CD5^+CD1d^+$ phenotype (**Fig. 5C, Fig. 6F and Supplementary Fig. 3F**)[26,61]

218 and the other a memory $CD27^+CD24^+$ phenotype [59](**Fig. 6G and Supplementary Fig. 3G**). The second

219 putative regulatory population also expressed PDL-1, the receptor for PD-1, important for regulating

220   the T cell response in TB [3,62,63]. The importance of antigen specific memory B cells and the PDL-1/PD-1

221   axis for localising T_FH cells within GrALT and mediating TB control in both mice and macaques was

222   recently demonstrated [3]. Together these flow cytometry data confirm the presence of diverse B cell

223   phenotypes in TB diseased lung tissue, including an expanded CD11c expressing atypical B cell

224   population, subsets potentially associated with GC activity, antibody production, and regulation.

225   **B cells impact *Mtb* growth in a 3D granuloma biomimetic model**

226   To investigate the potential effect of B cells on *Mtb* growth, we turned to a 3D biomimetic culture

227   model that resembles the granuloma microenvironment [64,65]. The model uses peripheral blood

228   mononuclear cells (PBMC) infected with bioluminescent *Mtb*. These *Mtb*-infected PBMC are then

229   encapsulated in collagen/alginate microspheres that contain an extracellular matrix scaffold. Each

230   microsphere therefore represents a 3D microenvironment that mimics an individual granuloma.

231   Without B cell depletion, the overall *Mtb* growth rate was significantly greater in the TB patient

232   derived undepleted PBMC versus the control samples, consistent with immune dysregulation during

233   TB disease (**Fig. 7A**). CD19^{+} B cells were depleted from PBMC using positive magnetic selection and

234   *Mtb* growth kinetics measured compared to non-depleted microspheres (**Fig. 7B**). Using PBMC from

235   four healthy donors, with each condition performed in triplicate, demonstrated that B cell depletion

236   caused a consistent and significant increase in *Mtb* growth (**Fig. 7C and D**). Interestingly though, the

237   effect of depletion on PBMC from patients with active TB prior to the initiation of drug therapy was

238   highly variable, with *Mtb* growth increasing in two of the donors and decreasing in the remaining two

239   (**Fig. 7D**). Together, these data demonstrate that B cells can regulate *Mtb* growth, but this effect is

240   variable in active TB suggesting their function can be altered by ongoing disease.

241   **Lung tissue derived antibodies show *Mtb* specificity and enhance bacterial phagocytosis**

242   Having observed an expansion of ASC subsets in TB diseased lung tissue, we compared the relative

243   frequency of ASCs of TB and non-TB-diseased patients and found an enrichment in lung tissue in both

244   groups (**Fig. 8A**). The ASCs expressed the tissue residence marker CD69 and the plasma cell marker

245 CD138 [27,37]. These compartmental differences prompted us to investigate the antibody profiles in TB

246 lungs. Therefore, we isolated antibodies from lung tissue homogenates using a thiophilic gradient (**Fig.**

247 **8B**)[66] and confirmed the presence of IgM, IgD, IgG and IgA (**Fig. 8C**; IgE was not detected). The purified

248 antibodies were reactive to whole *Mtb* lysate by ELISA, and significantly enriched in the TB diseased

249 patients (**Fig. 8D**). Although individual *Mtb*-reactive antibody classes showed similar upregulation,

250 only IgM was significantly upregulated in the TB diseased patients (**Fig. 8E**).Interestingly, in this highly

251 TB endemic population, there was no difference in the reactivity of plasma derived antibodies from

252 the same TB and non-TB diseased participants (**Supplementary Figure 4**). These data indicate the

253 enrichment of TB specific antibodies in TB diseased human lung tissue, supporting a role at the site of

254 disease.

255 Finally, to confirm the specificity of these antibodies and to test their functionality, purified antibodies

256 were studied using the 3D biomimetic *Mtb* culture model [65]. Antibodies purified from lung

257 homogenate of TB diseased participants enhanced the phagocytosis of *Mtb*, shown by increased

258 uptake of luminescent *Mtb* compared to isotype controls (**Fig. 8F**). Although the flow cytometry does

259 not determine if the bacteria are phagocytosed or cell-associated, the cells are extensively washed

260 post-infection, and we have previously shown that *Mtb* growth in this system is predominantly

261 intracellular [64]. Subsequent growth of *Mtb* over the next two weeks was markedly greater when *Mtb*

262 had been treated with these antibodies (**Fig. 8G**). However, when the results were normalized to the

263 initial infectious load, no significant change in the growth rate was observed, suggesting the antibodies

264 do not modulate subsequent proliferation, at least within this model system (**Fig. 8H**). Thus, these

265 data confirm the presence of *Mtb* specific antibodies in TB affected lung tissue, which enhance the

266 phagocytosis of mycobacteria.

267

268

269

270 **Discussion**

271 Diverse lines of evidence, from human studies and animal models, demonstrate that B cells are

272 involved in the host response to *Mtb*, but B cells represent a multi-faceted immune subset, and their

273 precise role has remained elusive. The frequency of B cells in circulation is reduced during active TB

274 [11,13-17] and infection is known to induce B cell containing tertiary lymphoid follicles in the lung referred

275 to as granuloma-associated lymphoid tissue (GrALT)[3,8,11,12]. Using matched blood and lung samples,

276 we show that these phenomena overlap, with decreased B cells in the blood reflecting an increase in

277 the lungs of human TB patients. Lung B cell frequency was extremely high in some participants, and,

278 by histology, they were found to be associated with the granuloma in similar quantities to T cells. We

279 next performed a detailed characterization of B cell phenotypes in human TB lung tissue using

280 complementary scRNAseq and flow cytometry approaches and interrogate the potential functional

281 impact in a cellular model. For technical reasons, it was not possible to perform scRNAseq analysis and

282 FACS analysis on the same samples, however, the fact that we observe similar changes at both the

283 transcriptional and protein level supports the phenotypic changes observed by each approach, despite

284 analysis being in different samples.

285 A central focus of our study was to compare B cells in the lung compartment with those in circulation,

286 which have been the focus of most studies in humans. In contrast to a predominantly naïve and

287 transitional phenotype in the blood, lung B cells were mostly of a memory and ASC phenotype and

288 expressed the tissue residence marker CD69, consistent with resident memory cells [67]. There is limited

289 data regarding human lung derived B cell phenotypes, but our data are supported by Barker *et al*. and

290 Tan *et al*., who also observed CD69^{+} expression [68,69]. Mechanistically, from mouse models, the

291 recruitment of B cells to the lung requires local antigen encounter [27,69,70]. The initial seeding of memory

292 B cells in the lung is derived from the mediastinal lymph node [69], with lung resident cells expressing

293 CXCR3, CCR6 and CD69 [27,69]. These cells patrol the lung and upon local antigen encounter either form

294 part of induced bronchus-associated lymphoid tissue (iBALT), or GrALT in the case of TB, or

295 differentiate into ASC [27,70]. We observed memory B cells and ASCs expressing all three markers,

296 supporting their tissue residence. Interestingly, Tan *et al*. detected a resting memory B cell phenotype

297 and little expression of GC-associated markers Bcl6, Ki67 and AICDA in healthy lungs [69]. In contrast, we

298 observed two memory B cell populations expressing these transcripts in our scRNAseq data, in

299 addition to a memory B cell phenotype expressing both CCR6 and CCR7 homing markers by flow

300 cytometry. We also detected both transcripts and surface expression of the plasma cell marker CD138.

301 Together, our findings reflect the diseased state of these TB patient lungs, suggestive of local antigen

302 encounter by B cells in the lung and their involvement in GrALT, with differentiation into ASCs and

303 hence a tissue resident B cell response.

304 Several of our findings point toward the possible function or interaction of B cells with T cells within

305 the GrALT. CCR7 facilitates migration of B cells toward the T cell zone within GC, allowing for B cell

306 help from T_FH cells [44,71] and a key interaction with T_FH cells includes the CD40-CD40L interaction [72], all

307 of which were expressed by lung B cells. Linge *et al*. demonstrate that B cells are an important source

308 of IL6 and that the T_H1 and T_H17 response [23] is affected when IL6 is knocked out of B cells [21]. Regarding

309 putative regulatory B cells observed in the lung, recent evidence suggests that antigen experienced

310 memory B cells expressing PDL-1 are important in recruiting T_FH cells into GC [3]. Moreover, Zhang *et*

311 *al*. show that $CD5^{hi}CD1d^+$ B cells can inhibit IL-17 production by T cells [26]. These cells were present in

312 TB diseased lung tissue and have previously been observed in circulation of patients with ATBI and

313 expanded in those with cavitation [25,32]. The local inflamed milieu of the lung is also reflected by the

314 presence of atypical B cells, which are associated with an inflamed state [51,53]. The atypical cells

315 expressed TLR2 and 4, of which the former could detect bacterial lipoprotein such as ManLAM for

316 example, resulting in MyD88 signaling and the IL8 response, which could result in the local recruitment

317 of immune cells including T cells [73,74]. Importantly, CD11c B cells have been associated with many

318 inflammatory conditions in humans including granulomatous lung diseases such as sarcoidosis [75]. In

319 that study, these were termed age-associated B cells (ABCs), which share the same markers and

320 probably represent the same or very similar B cell populations [76]. In addition, atypical or ABC are

321 associated with many autoimmune conditions including Lupus and multiple sclerosis, and TB disease

322 shares clinical similarities with such autoimmune conditions [77,78]. It is possible, therefore, that the

323 atypical B cells enriched in TB diseased lungs play a role in the immunopathogenesis of TB, through

324 mechanisms including antibody and cytokine production and cross talk with T cells. Overall, the

325 heterogeneity of B cells observed in TB diseased lung tissue is consistent with multiple putative roles

326 in TB protection and pathogenesis. We do concede that these data are only descriptive of the array of

327 B cells found in the human TB lung, and specific functional roles remain to be mechanistically proven.

328 To investigate the effect of B cells on *Mtb* in the lung, we used a granuloma biomimetic model and

329 found that depletion of B cells increases *Mtb* growth. This is consistent with mouse [6,7] and NHP [10]

330 studies showing an increased pulmonary bacterial burden in the absence of B cells. In addition, Joosten

331 *et al*. observed a negative correlation between B cell frequency and bacterial growth in humans, using

332 a whole blood mycobacterial growth inhibition assay [79]. Consequently, all these studies support a

333 protective role for B cells, but notably in our model this control is inconsistent when PBMCs from

334 patients with active TB were used. We believe it is likely to reflect the fact that the TB patients were,

335 by chance, at very different stages of disease severity. For example, in more severe TB disease we

336 expect higher frequencies of pro-inflammatory atypical B cells, which may contribute to *Mtb* growth.

337 The depletion of B cells in these cases may reduce *Mtb* growth, both in the 3D model and by analogy,

338 in the lung. This is supported by the fact that *Mtb* growth was higher in PBMCs from TB patient's vs

339 controls before B cell depletion (**Fig.7A**). However, additional experiments are required to explore this

340 hypothesis further. This suggests that B cells can contribute to control of *Mtb* growth, but also that

341 the B cell compartment is disrupted during active TB. In a longitudinal study, Moreira-Teixeira *et al*.

342 observed a decreased B cell signature with increased disease progression in the blood of LTBI patients,

343 LTBI-progressors and ATBI patients, consistent with our observation [16]. Similarly, several studies

344 showed that the proportions of B cell populations and transcriptional signatures are affected by TB

345 [11,15,16,80].

346   Finally, we analyzed the antibodies present in TB-affected lung tissue and found significantly increased

347   levels of those specific for *Mtb*. This was observed for all antibody classes, but only reached

348   significance for IgM. Interestingly, IgM is known to be a potent activator of the complement system,

349   which is a strong biomarker of TB disease [81]. In addition, IgM memory B cells are associated with

350   induced lymphoid tissue in mucosal barriers [82], suggesting a potential link with the GrALT observed in

351   TB affected lungs. IgM memory B cells are emerging as important effectors of both adaptive and

352   innate-like immune responses in mucosal barriers [82]. Antibodies from the lungs of infected patients

353   enhanced uptake of *Mtb,* confirming both specificity and consistent with opsonisation increasing

354   phagocytosis of mycobacteria [83]. However, we did not detect an effect on subsequent *Mtb* growth in

355   our granuloma biomimetic model. A strong IgM response was associated with protection against TB

356   disease in NHPs vaccinated with BCG via an intravenous route [84]. In addition, studies in humans have

357   shown enhanced phagocytosis, phagolysosome fusion and macrophage killing using plasma

358   antibodies isolated from TB resistors compared to those with active TB disease [29,85]. As lung antibodies

359   used in this study were isolated from subjects with advanced TB lung disease, it is therefore perhaps

360   expected that they failed to reduce *Mtb* growth despite enhanced phagocytosis. However, the fact

361   that TB specific antibodies are present at the site of disease in humans supports a role in the immune

362   response to *Mtb* infection in humans.

363   **Conclusion**

364   B cell phenotype and function differs significantly between the lung and circulation, and B cells can

365   regulate the host-pathogen interaction in TB. B cells isolated from human lung tissue displayed unique

366   phenotypic subsets including populations consistent with tissue resident memory, GC activity, atypical

367   and regulatory B cells, suggesting potentially diverse roles in the immune response to *Mtb*. In addition,

368   *Mtb*-specific antibodies are enriched in TB diseased lung tissue and augment phagocytosis of *Mtb*.

369   These data show B cells are likely to contribute to the host response to TB in humans at multiple points

370   and highlight that considering tissue-specific phenotypes is likely to be essential to fully understand

371   their overall impact. Future studies will aim to assess the TB specificity of the B cells in the GrALT and

372   focus on spatial transcriptomic approaches to investigate the nature of the B cell follicles within the

373   lung and if they form part of protection or pathology.

374

375   **Methods**

376   **Cohort description**

377   This study made use of a cohort of patients that underwent thoracotomy or lung resection surgeries.

378   This included patients with a history of TB and non-TB associated pathologies, with or without HIV.

379   Written informed consent was obtained from all enrolled participants and surgeries were performed

380   at either the King Dini-Zulu Hospital Complex or Inkosi Albert Luthuli hospital in Durban, KwaZulu-

381   Natal, South Africa. Patients were assessed for the extent of lung disease (cavitation and/or

382   bronchiectasis) via HRCT. Candidates for surgery had to pass a fitness test as determined by Karnofsky

383   score, six minute walk test, spirometry, and arterial blood gas. Patients with massive hemoptysis were

384   further assessed for their general condition, effort tolerance prior to hemoptysis, arterial blood gas

385   measurement, serum albumin level and HRCT imaging. Tissues were collected following surgery to

386   remove the irreversibly damaged lobes or lungs. Resected lung tissue was dissected into smaller tissue

387   samples on site and transferred to RPMI 1640 media containing 10% FBS and kept on ice. The sections

388   selected for analysis represented visibly low-, mid- and severely diseased areas of the lung, which

389   were combined and processed[86]. Therefore, the isolated cells were representative of the entire lung

390   and were not necessarily only of granulomatous origin. Samples were received for processing within

391   one hour of dissection and processed immediately in a BSL3 facility.

392

393

394

16

395 **Table 1: Descriptive table of the study cohort (n=76):**

	Gender	+ Lymph node	HIV +ve	TB	Smokers	Age*
Male	47 (62%)	7	20 (43%)	34 (72%)	21 (45%)	42 (35-48)
Female	29 (38%)	10	19 (66%)	24 (83%)	1 (3%)	39 (34,47)
Total	**76**	**17**	**39 (51%)**	**58 (76%)**	**22 (29%)**	

396

397 * Median and IQR are indicated

398 The cohort consisted largely of a Black African population 82% (90% of males and 74% of females). A

399 total of 76 lung samples were collected, including 17 lung draining lymph nodes and all samples with

400 matched blood. About half of the cohort was HIV positive, with positivity skewing slightly toward

401 females. Most resections were TB-related (76%), with a median age of 41 years, and a relatively similar

402 age distribution amongst males and females. Close to two thirds of cases were males, and of these

403 45% were active/previous smokers. Lung cancer resections were dissected, and the healthy tissue

404 margins were retained as the TB-negative control lung samples[86].

405 **Histology**

406 A section of lung was cut and transferred to 10% buffered formalin to fix. The sample was then

407 processed in a vacuum filtration processor using a xylene-free method and isopropanol as the main

408 substitute fixative. The tissues were embedded in paraffin wax and then cut into 4 μm sections, baked

409 at 60°C for 15 min, dewaxed using two xylene changes and rehydrated with descending grades of

410 alcohol to water. These were then Hematoxylin and Eosin (H&E) stained using standard procedures,

411 then dehydrated again in ascending grades of alcohol, cleared in xylene and mounted with a distyrene,

412 plasticizer and xylene solution (DPX). The H&E slides were used to assess specimen quality before

413 proceeding to immunohistochemistry.

414 Tissue sections (4 μm) of specimens of good quality were mounted on charged slides, and heated at

415 56° C for 15 min. Sections were dewaxed in xylene, rinsed in 100% ethanol and one change of SVR

416 (95%), washed under running water for two minutes followed by antigen retrieval via Heat Induced

417 Epitope Retrieval (HIER) in Tris-HCl (pH 6.0) for 30 minutes. Slides were cooled for 15 minutes and

418 rinsed under running water for two minutes. Endogenous peroxide activity was blocked using 3% H_2O_2

419 for 10 minutes at room temperature (RT), followed by a wash in PBST and blocking with protein block

420 (Novolink) for 5 minutes at RT. Slides were incubated with primary antibodies for CD20 (M0755-

421 CD20cy-L26, DAKO), CD68 (ab192847, Abcam), CD45 (M0701-2B11+PD7/26, DAKO), CD3

422 (ab16669,Abcam) and CD21 (M0784-1F8, Dako), followed by washing and incubation with the

423 polymer (Novolink) for 30 minutes at RT. Finally, the slides were washed and stained with

424 diaminobenzidine (DAB) for 5 minutes, washed and counterstained with hematoxylin for 2 minutes,

425 washed and blued in 3 % ammoniated water for 30 seconds, washed, dehydrated, and mounted in

426 DPX. Slides were imaged using a Hamamatsu NDP slide scanner (Hamamatsu NanoZoomer RS2, Model

427 C10730-12) and its viewing software (NDP.View2). The red, green, and blue color balance was kept at

428 100% whereas gamma correction was maintained between 0.7 and 2. Brightness (60–110%) and

429 contrast (100–180%) settings varied slightly between slides depending on staining quality. Resolution

430 was 230 nm/pixel yielding file sizes of 2-4.4 GB. Contrast, brightness, and intensity of exported images

431 (jpg format) were minimally adjusted using CorelDraw 2020. DAB stained cells were quantified using

432 QuPath (https://qupath.github.io/) with the operator blinded to the nature of the sample.

433 **Peripheral blood mononuclear cell (PBMC) isolation**

434 Blood samples were collected into EDTA tubes and processed within four hours of collection. Samples

435 were centrifuged 930 x g for 5 minutes and 1 ml plasma fractions were aliquoted and stored at -80°C.

436 The remaining red blood cell pellet was made up to three times its pellet volume with PBS warmed to

437 room temperature. PBMCs were isolated using a Ficoll-Paque (Amersham Biosciences, Little Chalfont,

438 UK) density gradient sedimentation method as per manufacturer's instructions. Isolated PBMCs were

439 cryopreserved in 10% DMSO in heat inactivated fetal bovine serum (FBS, ThermoFischer Scientific)

440 and stored in liquid nitrogen until use.

441

Lung mononuclear cell (LMC) isolation

Tissue specimens were mechanically dissociated using scissors followed by GentleMACs (Miltenyi Biotec) homogenization for 15 seconds in RPMI 1640, 10% FBS, 40 μg collagenase D (Roche) and 40 U/ml DNAse I (SIGMA-Aldrich). Samples were then incubated for 30 minutes at 37°C, followed by another 75 second homogenization cycle and passed through 70 μm cell strainer (Corning). Following a five min 930 x g centrifugation (Beckman Coulter, Allegra X-12R), the sample pellet was suspended in 5 ml and passed through a 40 μm cell strainer and centrifuged as before. Finally, the pellet was treated with 5 ml red blood cell lysis solution (QIAGEN) for 5 minutes, made up to 30 ml with PBS and centrifuged again. Cells were counted and split into equal numbers (1 - 5 million) to stain for flow cytometry. Lung draining lymph nodes were processed similarly without the need for GentleMACs homogenization or collagenase D and DNAse I treatment.

Flow cytometry

Isolated LMCs were processed for flow cytometry on the same day to avoid reduced viability following cryopreservation and thawing. To facilitate running matched blood samples on the same day as stained LMCs, isolated PBMCs were thawed on the day the lung samples were processed. Briefly, cryopreserved PBMCs were thawed, washed, and rested in RPMI 1640 containing 10% FBS for one hour in a 37°C, 5% CO_2 incubator prior to staining. Between 1 - 5 million PBMCs or LMCs were stained with the respective B cell surface marker panels (**Supplementary Tables 1 to 3**) for 20 minutes at RT in the dark. Samples were washed twice with PBS and suspended in 250 μl 2% PFA-PBS and kept at 4°C in the dark. Samples were acquired on a BD FACS Aria Fusion III and data analyzed using FlowJo version 9.9.6 (Tree Star).

466   **Supplementary Table 1: B cell maturation panel**

Marker	Fluorochrome	Clone	Cat. no	Supplier	Dilution factor	Host
L/D	APC-Cy7		L10119	Invitrogen	200	
CD45	APC	HI30	304012	BioLegend	25	mouse
CD3	Bv711	OKT3	317328	BioLegend	50	mouse
CD14	Bv711	M5E2	301838	BioLegend	25	mouse
CD19	Bv605	HIB19	302244	BioLegend	50	mouse
CD27	Bv510	O323	302836	BioLegend	50	mouse
CD38	PECy7	HIT2	303516	BioLegend	50	mouse
IgM	PerCP/Cy5.5	MHM-88	314512	BioLegend	100	mouse
IgD	AF700	IA6-2	348230	BioLegend	25	mouse
CD138	Bv785™	MI15	356538	BioLegend	25	mouse
CXCR5	AF488	RF8B2	558112	BD Pharmingen	100	rat
CD11c	PE	S-HCL-3	371504	BioLegend	25	mouse
CD95 (Fas)	Bv650™	DX2	305642	BioLegend	50	mouse
CD20	PE/Dazzle™ 594	2H7	302348	BioLegend	50	mouse
CD69	BUV395	FN50	564364	BD Horizon	100	mouse
CD10	PE-Cy5	HI10a (RUO)	555376	BD Pharmingen	10	mouse
CD21	Bv421	B-ly4	562966	BD Horizon	100	mouse
CD40	BUV496	5C3	741159	BD OptiBuild	50	mouse

467

468   **Supplementary Table 2: B cell homing panel**

Marker	Fluorochrome	Clone	Cat. no	Supplier	Dilution factor	Host
L/D	APC-Cy7		L10119	Invitrogen	200	
CD45	APC	HI30	304012	BioLegend	25	mouse
CD3	Bv711	OKT3	317328	BioLegend	50	mouse
CD14	Bv711	M5E2	301838	BioLegend	25	mouse
CD19	Bv605	HIB19	302244	BioLegend	50	mouse
CD27	Bv510	O323	302836	BioLegend	50	mouse
CD38	PECy7	HIT2	303516	BioLegend	50	mouse
IgM	PerCP/Cy5.5	MHM-88	314512	BioLegend	100	mouse
IgD	AF700	IA6-2	348230	BioLegend	25	mouse
CCR6 (CD196)	Bv421	GO34E3	353439	BioLegend	25	mouse
CXCR5	AF488 (FITC)	RF8B2	558112	BD Pharmingen	100	rat
CXCR4 (CD184)	Bv785™	12G5	306530	BioLegend	50	mouse
CD62L	PE-Cy5	DREG-56	555545	BD Pharmingen	50	mouse
CXCR3 (CD183)	PE-CF594	IC6/CXCR3	562451	BD Horizon	25	mouse
CD69	BUV395	FN50	564364	BD Horizon	100	mouse
CCR7	PE	150503	FAB197P	R&D Biosystems	25	mouse

469

470

471

472

473 **Supplementary Table 3: B cell regulatory panel**

Marker	Fluorochrome	Clone	Cat. no	Supplier	Dilution factor	Host
L/D	APC-Cy7		L10119	Invitrogen	200	
CD45	APC	HI30	304012	BioLegend	25	mouse
CD3	Bv711	OKT3	317328	BioLegend	50	mouse
CD14	Bv711	M5E2	301838	BioLegend	25	mouse
CD19	Bv605	HIB19	302244	BioLegend	50	mouse
CD38	PECy7	HIT2	303516	BioLegend	50	mouse
IgM	PerCP/Cy5.5	MHM-88	314512	BioLegend	100	mouse
IgD	AF700	IA6-2	348230	BioLegend	25	mouse
CD27	PE-Cy5	1A4CD27	6607107	Beckman Coulter	25	mouse
CD40	BUV496	5C3	741159	BD OptiBuild	50	mouse
PD-L1 (CD274)	PE	29E.2A3	329706	BioLegend	50	mouse
CD24	FITC	ML5	311104	BioLegend	25	mouse
CD178 (Fas-L)	Bv421™	NOK-1	306412	BioLegend	10	mouse
CD1d	Bv510™	51.1	350314	BioLegend	10	mouse
CD5	PE/Dazzle™ 594	L17F12	364012	BioLegend	50	mouse
CD86	Bv650™	IT2.2	305428	BioLegend	50	mouse

474

475 **Lung homogenate and plasma antibody isolation**

476 All homogenate supernatants throughout the LMC isolation protocol were reserved for isolation of

477 patient lung derived immunoglobulins. The homogenate supernatants were centrifuged at 10000 RCF

478 for 10 minutes to pellet any remaining cellular debris. These were then filtered through a 0.22 µm

479 syringe filter (Millipore, Merck). This clarified supernatant was then incubated with a Thiophilic resin

480 (Pierce, ThermoFischer) for isolation of immunoglobulins [66]. For plasma antibodies, 2 ml plasma was

481 loaded onto a thiophilic resin. Each sample type had a designated thiophilic column to avoid cross

482 contamination of purified immunoglobulin pools. Both sample types were incubated with the resin

483 for 1 hour at room temperature, after which the bound immunoglobulins were eluted as per the

484 manufacturer's instructions. The resulting eluted sample absorbance was measured at 280 nm and

485 fractions of interest were run on SDS-PAGE and Western blot to assess sample purity, after which they

486 were pooled by sample type. Sterile glycerol was added to 50% (v/v) and the pooled samples were

487 stored at -20°C.

488

SDS-PAGE and Western blot of isolated immunoglobulins

Isolated immunoglobulin fractions were prepared for analysis on 12.5% reducing SDS-PAGE gels [87]. Samples were prepared in an equal volume of reducing SDS-PAGE sample buffer containing 10% (v/v) β-mercaptoethanol and boiled for 5 minutes before loading on duplicate SDS-PAGE gels. Once completed, one gel was stained with Coomassie brilliant blue R250 (SIGMA) as a reference gel, whilst the second was transferred (Trans-Blot Turbo, Bio-Rad) to nitrocellulose membrane for Western blotting. PBS with 0.1% Tween-20 (PBST) was used throughout for Western blotting. Membranes were blocked with 5% low fat milk powder in PBST for 1 hour, washed twice with PBST and incubated with immunoglobulin class-specific primary antibodies (all at 1:5000 dilution) for 2 hours: Goat anti-human IgD-HRPO (cat. no 2030-05, Southern Biotech), Goat anti-human IgA-HRPO (cat. no 2050-05, Southern Biotech), Donkey anti-human IgG-HRPO (cat. no 709-036-073, Jackson ImmunoResearch), Donkey anti-human IgM-HRPO (cat. no 709-036-098, Jackson ImmunoResearch). Blots were washed again with PBST followed by a final wash and detection with enhanced chemiluminescence substrate (Pierce, ThermoFischer) using a ChemiDoc™ imager (Bio-Rad).

ELISA to test *Mtb* specificity of isolated immunoglobulins

Mycobacterium tuberculosis (*Mtb*) H37Rv cultures were used to prepare a lysate for ELISAs. The *Mtb* lysate protein concentration was determined by Pierce 660 nm protein assay (Pierce, ThermoFischer) and used to coat ELISA plates at 10 µg/ml of lysate in PBS, 100 µl/well overnight at 4°C. Plates were washed three times between each incubation step, using 200 µl/well PBS with 0.1% Tween-20 (PBST). The ELISA plate wells were blocked with 0.5% BSA in PBST for 1 hour at 37°C. This was followed by adding either the plasma or lung isolated immunoglobulins at a starting concentration of 100 µg/ml, 100 µl/well and serially diluting at 1:5, giving a final range from 100 to 0.8 µg/ml. Plates were incubated for 1 hour at 37°C. Finally, the plates were incubated for 1 hour at 37°C with the class-specific secondary antibodies as described for the Western blotting protocol and detected using TMB

substrate. The final titration curves were compared between samples as Area Under the Curve (AUC) readouts.

Mycobacterium tuberculosis (Mtb) culture

Standard *Mtb* H37Rv and bioluminescent *Mtb* H37Rv [88] cultures were maintained in Middlebrook 7H9 medium (Difco) supplemented with 10% OADC, 0.2% glycerol, 0.01% Tyloxapol (SIGMA). For the bioluminescent H37Rv *Mtb* the media was supplemented with 25 µg/ml kanamycin. Cultures were grown to 1×10^8 CFU/ml *Mtb* (OD = 0.6) at which point they were suitable for infections using a multiplicity of infection (M.O.I.) of 0.1.

Bio-electrospray (BES) 3D culture biomimetic model

A 3D culture biomimetic model, designed to mimic the host-pathogen interaction [64,89], was used to assess the impact of B cell depletion or antibody supplementation on the growth of *Mtb*.

Freshly isolated PBMCs were used for the BES experiments. Cells were infected with *Mtb* overnight in a T75 flask whereafter they were detached, washed, and mixed with 1.5% sterile alginate (Pronova UP MVG alginate, Nova Matrix) with human collagen (Advanced BioMatrix) to give a final concentration of 5×10^6 cells/ml. The PBMCs were encapsulated using an electrostatic bead generator (Nisco, Zurich, Switzerland) at a 10 ml/hr flow rate using a Harvard syringe fitted with a 0.7 mm external diameter nozzle and dropping into a 100 mM $CaCl_2$ ionotropic HBSS gelling bath as described in detail by Tezera *et al.* [64,89]. The resulting ~600 µm diameter microspheres containing the *Mtb* infected PBMCs were washed twice with HBSS with Ca^{2+}/Mg^{2+} and transferred to RPMI 1640 supplemented with 10% human AB serum, 25 µg/ml kanamycin, 1% ampicillin. The beads were transferred to Eppendorffs and incubated at 37 °C, 5 % CO_2. The use of a bioluminescent *Mtb* allowed growth to be monitored using a luminometer (GloMax 20/20 Luminometer, Promega), with readings taken every 2 - 3 days over a 15 day period.

536 The initial set of BES experiments involved a B cell depletion step using a EasySep™ CD19 positive

537 selection kit II (STEMCELL), with the control PBMCs remaining "untouched". B cell depletion was

538 performed prior to *Mtb* infection as described above. To confirm the CD19 depletion efficacy, samples

539 were stained with a basic flow cytometry antibody panel, using L/D, CD45, CD3 and CD19 antibodies

540 as listed in **Supplementary Table 1**. Cultures were maintained for a total of 15 days post infection and

541 luminescence was measured every two to three days.

542 For the second set of BES experiments, PBMCs were left untouched, however, *Mtb* was treated with

543 the antibodies or control non-specific human IgG (SIGMA, cat. 56834-25mg) for one hour prior to

544 infection of the PBMCs overnight and a media-only control was included. Relative infectivity was

545 measured immediately, or cultures within microspheres were maintained for 15 days, and

546 luminescence was measured as before.

547 **Seq-Well single cell RNA sequencing**

548 LMCs were prepared for seq-well as previously described [90]. Cells were diluted to a single cell

549 suspension of 15 000 cells in 200 µl RPMI, 10% FBS and loaded onto a polymethylsiloxane (PDMS)

550 array pretreated with R10 media for 15 minutes. Once the cells settled into the microwells, the

551 microarray was washed with PBS (SIGMA) then sealed with a plasma functionalized polycarbonate

552 membrane (Sterlitech). The sealed arrays were incubated at 37°C for 40 minutes, followed by 20

553 minutes at room temperature in a guanidinium thiocyanate (SIGMA), EDTA (ThermoFischer), 1% β-

554 mercaptoethanol (SIGMA) and sarkosyl (SIGMA) buffer. Capture beads were then allowed to hybridize

555 with released mRNA in a hybridization PBS, NaCl (ThermoFischer), $MgCl_2$ (SIGMA) and polyethylene

556 glycol (PEG) (SIGMA) buffer, with gentle shaking at 60 rpm for 40 minutes. The beads with the

557 captured mRNA were collected from the wells with three washes of a Tris-HCl (ThermoFischer) buffer

558 containing NaCl and $MgCl_2$ and centrifugation at 2500 x g for 5 min after each wash.

559 cDNA synthesis was done in a mastermix containing Maxima H Minus Reverse Transcriptase, Maxima

560 buffer, dNTPs, RNAse inhibitor, a template switch oligonucleotide and PEG for 30 minutes at room

561 temperature, followed by an overnight incubation at 52°C with end-over-end mixing. The cDNA was

562 digested with exonuclease and complementary DNA denatured from the capture beads with a 5

563 minute incubation in NaOH (SIGMA) and a wash with Tris-HCl, EDTA and Tween-20 (ThermoFischer).

564 PCR amplification was then performed following suspension of the beads in a mastermix containing

565 Klenow Fragment (NEB), dNTPs, PEG and dN-SMRT oligonucleotide and incubating for 45 min at 38°C.

566 Hereafter the PCR product was cleaned twice with an AMPure XP SPRI (Agencourt) bead cleanup at

567 0.6 and 0.8 times sample volume ratios. The product quality was assessed by Agilent Tape station

568 hsD5000, confirming an expected 1 kbp amplicon with little or no primer dimers below 200 bp. The

569 DNA libraries were quantified (Qubit High Sensitivity DNA kit) before preparation for Illumina

570 sequencing using the Nextera XT DNA sample preparation kit, with 900 pg of each library added to the

571 tagmentation reaction. The amplified product was cleaned again using the AMPure XP SPRI beads and

572 the final libraries pooled before loading onto the NovaSeq 6000 using a paired end read structure with

573 a read 1 primer: read 1:20 bases, read 2: 50 bases, read 1 index: 8 bases.

574 The sequencing reads were analyzed by aligning them to the hg19 genome assembly and processing

575 them according to the Drop-Seq Computation Protocol v2.0 (https://github.com/broadinstitute/Drop-

576 seq). This yields a cell by gene matrix which was then transformed to $\log_e$(UMI+1) using the Seurat R

577 package v3.1.0 (https://satijalab.org/seurat/) and scaled by a factor of 10000. The overall quality was

578 assessed by the read distribution, the number of transcripts, and genes per cell. A Uniform Manifold

579 Approximation and Projection (UMAP) was used for dimensionality reduction with the min distance

580 set to 0.5 and the neighbors set to 30. To cluster cells with similar transcriptional profiles, an

581 unsupervised clustering algorithm, FindClusters, was used with the resolution set to 0.5. These clusters

582 were then further divided using a differential expression test, FindAllMarkers, in Seurat, setting

583 "test.use" to "wilcox", Wilcoxon-adjusted p value cutoff < 0.01.

584

585

Statistical analysis

All analyses, except for Seqwell data, were performed in Prism (v9; GraphPad Software Inc., San Diego, CA, USA). Nonparametric tests were used throughout, with Mann-Whitney and Wilcoxon tests used for unmatched and paired samples, respectively and a three way ANOVA, Kruskal-Wallis comparison. *P* values less than 0.05 were considered statistically significant and denoted by * ≤ 0.05; ** < 0.01; *** < 0.001 and **** < 0.0001.

Study approval

Human patients undergoing thoracotomy or lung resection surgery for TB or non-TB associated pathologies gave written informed consent for a blood draw and tissue collection. The study protocol, data collection tools and associated consent forms were approved by the University of KwaZulu-Natal Biomedical Research Ethics Committee (BE 019/13). The CUBS study protocol for blood collection from healthy donors and patients with active TB was also approved (BE 022/13). Healthy blood donor study ethical approval was provided by the National Research Ethics Service Committee South Central — Southampton A, ref 13/SC/0043, Southampton, United Kingdom. Participant compensation was approved by the relevant ethics committees.

Data availability

The original contributions presented in the study are included in the article/Supplementary Material. Further inquiries can be directed to the corresponding author.

References

609

610   1.   Organization, W.H. Global tuberculosis report 2022. (2022).

611   2.   O'Garra, A.*, et al.* The immune response in tuberculosis. *Annu Rev Immunol* **31**, 475-527
612   (2013).

613   3.   Swanson, R.V.*, et al.* Antigen-specific B cells direct T follicular-like helper cells into lymphoid
614   follicles to mediate Mycobacterium tuberculosis control. *Nat Immunol* **24**, 855-868 (2023).

615   4.   Choreno-Parra, J.A.*, et al.* Mycobacterium tuberculosis HN878 Infection Induces Human-Like
616   B-Cell Follicles in Mice. *J Infect Dis* **221**, 1636-1646 (2020).

617   5.   Hertz, D., Dibbern, J., Eggers, L., von Borstel, L. & Schneider, B.E. Increased male
618   susceptibility to Mycobacterium tuberculosis infection is associated with smaller B cell
619   follicles in the lungs. *Sci Rep* **10**, 5142 (2020).

620   6.   Linge, I., Kondratieva, E. & Apt, A. Prolonged B-Lymphocyte-Mediated Immune and
621   Inflammatory Responses to Tuberculosis Infection in the Lungs of TB-Resistant Mice. *Int J*
622   *Mol Sci* **24**(2023).

623   7.   Maglione, P.J., Xu, J. & Chan, J. B cells moderate inflammatory progression and enhance
624   bacterial containment upon pulmonary challenge with Mycobacterium tuberculosis. *J*
625   *Immunol* **178**, 7222-7234 (2007).

626   8.   Slight, S.R.*, et al.* CXCR5(+) T helper cells mediate protective immunity against tuberculosis. *J*
627   *Clin Invest* **123**, 712-726 (2013).

628   9.   Esaulova, E.*, et al.* The immune landscape in tuberculosis reveals populations linked to
629   disease and latency. *Cell Host Microbe* **29**, 165-178 e168 (2021).

630   10.   Phuah, J.*, et al.* Effects of B Cell Depletion on Early Mycobacterium tuberculosis Infection in
631   Cynomolgus Macaques. *Infect Immun* **84**, 1301-1311 (2016).

632   11.   Joosten, S.A.*, et al.* Patients with Tuberculosis Have a Dysfunctional Circulating B-Cell
633   Compartment, Which Normalizes following Successful Treatment. *PLoS Pathog* **12**, e1005687
634   (2016).

635   12.   Ulrichs, T.*, et al.* Human tuberculous granulomas induce peripheral lymphoid follicle-like
636   structures to orchestrate local host defence in the lung. *J Pathol* **204**, 217-228 (2004).

637   13.   Corominas, M.*, et al.* B-lymphocytes and co-stimulatory molecules in Mycobacterium
638   tuberculosis infection. *Int J Tuberc Lung Dis* **8**, 98-105 (2004).

639   14.   Hernandez, J.*, et al.* Low number of peripheral blood B lymphocytes in patients with
640   pulmonary tuberculosis. *Immunol Invest* **39**, 197-205 (2010).

641   15.   Roy Chowdhury, R.*, et al.* A multi-cohort study of the immune factors associated with M.
642   tuberculosis infection outcomes. *Nature* **560**, 644-648 (2018).

643   16.   Moreira-Teixeira, L.*, et al.* Mouse transcriptome reveals potential signatures of protection
644   and pathogenesis in human tuberculosis. *Nat Immunol* **21**, 464-476 (2020).

645   17.   La Manna, M.P.*, et al.* Impact of Mycobacterium tuberculosis Infection on Human B Cell
646   Compartment and Antibody Responses. *Cells* **11**(2022).

647   18.   du Plessis, W.J., Keyser, A., Walzl, G. & Loxton, A.G. Phenotypic analysis of peripheral B cell
648   populations during Mycobacterium tuberculosis infection and disease. *J Inflamm (Lond)* **13**,
649   23 (2016).

650   19.   Bosio, C.M., Gardner, D. & Elkins, K.L. Infection of B cell-deficient mice with CDC 1551, a
651   clinical isolate of Mycobacterium tuberculosis: delay in dissemination and development of
652   lung pathology. *J Immunol* **164**, 6417-6425 (2000).

653   20.   Chen, Y.*, et al.* B cells promote granulomatous inflammation during chronic Mycobacterium
654   tuberculosis infection in mice. *PLoS Pathog* **19**, e1011187 (2023).

655   21.   Linge, I.*, et al.* Pleiotropic Effect of IL-6 Produced by B-Lymphocytes During Early Phases of
656   Adaptive Immune Responses Against TB Infection. *Front Immunol* **13**, 750068 (2022).

657   22.   Darrah, P.A.*, et al.* Prevention of tuberculosis in macaques after intravenous BCG
658   immunization. *Nature* **577**, 95-102 (2020).

23. Darrah, P.A.*, et al.* Airway T cells are a correlate of i.v. Bacille Calmette-Guerin-mediated protection against tuberculosis in rhesus macaques. *Cell Host Microbe* **31**, 962-977 e968 (2023).

24. Zhang, M.*, et al.* B cell infiltration is associated with the increased IL-17 and IL-22 expression in the lungs of patients with tuberculosis. *Cell Immunol* **270**, 217-223 (2011).

25. Zhang, M.*, et al.* Anti-tuberculosis treatment enhances the production of IL-22 through reducing the frequencies of regulatory B cell. *Tuberculosis (Edinb)* **94**, 238-244 (2014).

26. Zhang, M.*, et al.* CD19(+)CD1d(+)CD5(+) B cell frequencies are increased in patients with tuberculosis and suppress Th17 responses. *Cell Immunol* **274**, 89-97 (2012).

27. MacLean, A.J.*, et al.* Secondary influenza challenge triggers resident memory B cell migration and rapid relocation to boost antibody secretion at infected sites. *Immunity* **55**, 718-733 e718 (2022).

28. Simmons, J.D.*, et al.* Immunological mechanisms of human resistance to persistent Mycobacterium tuberculosis infection. *Nat Rev Immunol* **18**, 575-589 (2018).

29. Lu, L.L.*, et al.* A Functional Role for Antibodies in Tuberculosis. *Cell* **167**, 433-443 e414 (2016).

30. Lu, L.L.*, et al.* IFN-gamma-independent immune markers of Mycobacterium tuberculosis exposure. *Nat Med* **25**, 977-987 (2019).

31. Kawahara, J.Y., Irvine, E.B. & Alter, G. A Case for Antibodies as Mechanistic Correlates of Immunity in Tuberculosis. *Front Immunol* **10**, 996 (2019).

32. Rijnink, W.F., Ottenhoff, T.H.M. & Joosten, S.A. B-Cells and Antibodies as Contributors to Effector Immune Responses in Tuberculosis. *Front Immunol* **12**, 640168 (2021).

33. Grace, P.S.*, et al.* Antibody Subclass and Glycosylation Shift Following Effective TB Treatment. *Front Immunol* **12**, 679973 (2021).

34. Ogongo, P.*, et al.* Tissue-resident-like CD4+ T cells secreting IL-17 control Mycobacterium tuberculosis in the human lung. *J Clin Invest* **131**(2021).

35. Gars, E., Butzmann, A., Ohgami, R., Balakrishna, J.P. & O'Malley, D.P. The life and death of the germinal center. *Ann Diagn Pathol* **44**, 151421 (2020).

36. Fischer, M.B.*, et al.* Dependence of germinal center B cells on expression of CD21/CD35 for survival. *Science* **280**, 582-585 (1998).

37. Clavarino, G.*, et al.* Novel Strategy for Phenotypic Characterization of Human B Lymphocytes from Precursors to Effector Cells by Flow Cytometry. *PLoS One* **11**, e0162209 (2016).

38. Day, S.*, et al.* Comparison of blood and lymph node cells after intramuscular injection with HIV envelope immunogens. *Front Immunol* **13**, 991509 (2022).

39. Tarte, K., Zhan, F., De Vos, J., Klein, B. & Shaughnessy, J., Jr. Gene expression profiling of plasma cells and plasmablasts: toward a better understanding of the late stages of B-cell differentiation. *Blood* **102**, 592-600 (2003).

40. Calame, K.L. Plasma cells: finding new light at the end of B cell development. *Nat Immunol* **2**, 1103-1108 (2001).

41. Xu, A.Q., Barbosa, R.R. & Calado, D.P. Genetic timestamping of plasma cells in vivo reveals tissue-specific homeostatic population turnover. *Elife* **9**(2020).

42. Lin, W.*, et al.* Circulating plasmablasts/plasma cells: a potential biomarker for IgG4-related disease. *Arthritis Res Ther* **19**, 25 (2017).

43. Gothel, S.F. & Marahiel, M.A. Peptidyl-prolyl cis-trans isomerases, a superfamily of ubiquitous folding catalysts. *Cell Mol Life Sci* **55**, 423-436 (1999).

44. Pereira, J.P., Kelly, L.M. & Cyster, J.G. Finding the right niche: B-cell migration in the early phases of T-dependent antibody responses. *Int Immunol* **22**, 413-419 (2010).

45. Bunting, K.L.*, et al.* Multi-tiered Reorganization of the Genome during B Cell Affinity Maturation Anchored by a Germinal Center-Specific Locus Control Region. *Immunity* **45**, 497-512 (2016).

709   46.   Lefebvre, C.*, et al.* A human B-cell interactome identifies MYB and FOXM1 as master
710   regulators of proliferation in germinal centers. *Mol Syst Biol* **6**, 377 (2010).

711   47.   Ranuncolo, S.M.*, et al.* Bcl-6 mediates the germinal center B cell phenotype and
712   lymphomagenesis through transcriptional repression of the DNA-damage sensor ATR. *Nat*
713   *Immunol* **8**, 705-714 (2007).

714   48.   Robbiani, D.F. & Nussenzweig, M.C. Chromosome translocation, B cell lymphoma, and
715   activation-induced cytidine deaminase. *Annu Rev Pathol* **8**, 79-103 (2013).

716   49.   Meyer, S.J.*, et al.* CD22 Controls Germinal Center B Cell Receptor Signaling, Which Influences
717   Plasma Cell and Memory B Cell Output. *J Immunol* **207**, 1018-1032 (2021).

718   50.   Salerno, F.*, et al.* An integrated proteome and transcriptome of B cell maturation defines
719   poised activation states of transitional and mature B cells. *Nat Commun* **14**, 5116 (2023).

720   51.   Jenks, S.A., Cashman, K.S., Woodruff, M.C., Lee, F.E. & Sanz, I. Extrafollicular responses in
721   humans and SLE. *Immunol Rev* **288**, 136-148 (2019).

722   52.   Jenks, S.A.*, et al.* Distinct Effector B Cells Induced by Unregulated Toll-like Receptor 7
723   Contribute to Pathogenic Responses in Systemic Lupus Erythematosus. *Immunity* **52**, 203
724   (2020).

725   53.   Woodruff, M.C.*, et al.* Extrafollicular B cell responses correlate with neutralizing antibodies
726   and morbidity in COVID-19. *Nat Immunol* **21**, 1506-1516 (2020).

727   54.   Krause, R.*, et al.* HIV skews the SARS-CoV-2 B cell response towards an extrafollicular
728   maturation pathway. *Elife* **11**(2022).

729   55.   Xin Gao, X.*, et al.* ZEB2 regulates the development of CD11c+ atypical B cells. *bioRxiv* (2022).

730   56.   Kang, S.M.*, et al.* MyD88 plays an essential role in inducing B cells capable of differentiating
731   into antibody-secreting cells after vaccination. *J Virol* **85**, 11391-11400 (2011).

732   57.   Georg, I., Diaz-Barreiro, A., Morell, M., Pey, A.L. & Alarcon-Riquelme, M.E. BANK1 interacts
733   with TRAF6 and MyD88 in innate immune signaling in B cells. *Cell Mol Immunol* **17**, 954-965
734   (2020).

735   58.   Muehlinghaus, G.*, et al.* Regulation of CXCR3 and CXCR4 expression during terminal
736   differentiation of memory B cells into plasma cells. *Blood* **105**, 3965-3971 (2005).

737   59.   Hasan, M.M.*, et al.* CD24(hi)CD38(hi) and CD24(hi)CD27(+) Human Regulatory B Cells Display
738   Common and Distinct Functional Characteristics. *J Immunol* **203**, 2110-2120 (2019).

739   60.   Scharer, C.D.*, et al.* Antibody-secreting cell destiny emerges during the initial stages of B-cell
740   activation. *Nat Commun* **11**, 3989 (2020).

741   61.   Yuan, C.*, et al.* Mycobacterium tuberculosis Mannose-Capped Lipoarabinomannan Induces
742   IL-10-Producing B Cells and Hinders CD4(+)Th1 Immunity. *iScience* **11**, 13-30 (2019).

743   62.   Ahmed, M., Tezera, L.B., Elkington, P.T. & Leslie, A.J. The paradox of immune checkpoint
744   inhibition re-activating tuberculosis. *Eur Respir J* **60**(2022).

745   63.   Tezera, L.B.*, et al.* Anti-PD-1 immunotherapy leads to tuberculosis reactivation via
746   dysregulation of TNF-alpha. *Elife* **9**(2020).

747   64.   Tezera, L.B.*, et al.* Dissection of the host-pathogen interaction in human tuberculosis using a
748   bioengineered 3-dimensional model. *Elife* **6**(2017).

749   65.   Reichmann, M.T.*, et al.* Integrated transcriptomic analysis of human tuberculosis granulomas
750   and a biomimetic model identifies therapeutic targets. *J Clin Invest* **131**(2021).

751   66.   Hutchens, T.W. & Porath, J. Thiophilic adsorption of immunoglobulins--analysis of conditions
752   optimal for selective immobilization and purification. *Anal Biochem* **159**, 217-226 (1986).

753   67.   Weisel, N.M.*, et al.* Comprehensive analyses of B-cell compartments across the human body
754   reveal novel subsets and a gut-resident memory phenotype. *Blood* **136**, 2774-2785 (2020).

755   68.   Barker, K.A.*, et al.* Lung-resident memory B cells protect against bacterial pneumonia. *J Clin*
756   *Invest* **131**(2021).

757   69.   Tan, H.X.*, et al.* Lung-resident memory B cells established after pulmonary influenza
758   infection display distinct transcriptional and phenotypic profiles. *Sci Immunol* **7**, eabf5314
759   (2022).

760 70. Allie, S.R.*, et al.* The establishment of resident memory B cells in the lung requires local
761   antigen encounter. *Nat Immunol* **20**, 97-108 (2019).
762 71. McHeik, S.*, et al.* Coexpression of CCR7 and CXCR4 During B Cell Development Controls
763   CXCR4 Responsiveness and Bone Marrow Homing. *Front Immunol* **10**, 2970 (2019).
764 72. Suan, D.*, et al.* CCR6 Defines Memory B Cell Precursors in Mouse and Human Germinal
765   Centers, Revealing Light-Zone Location and Predominant Low Antigen Affinity. *Immunity* **47**,
766   1142-1153 e1144 (2017).
767 73. Kunsch, C. & Rosen, C.A. NF-kappa B subunit-specific regulation of the interleukin-8
768   promoter. *Mol Cell Biol* **13**, 6137-6146 (1993).
769 74. Sims-Mourtada, J.C.*, et al.* In vivo expression of interleukin-8, and regulated on activation,
770   normal, T-cell expressed, and secreted, by human germinal centre B lymphocytes.
771   *Immunology* **110**, 296-303 (2003).
772 75. Phalke, S.*, et al.* Age-associated B Cells Appear in Patients with Granulomatous Lung
773   Diseases. *Am J Respir Crit Care Med* **202**, 1013-1023 (2020).
774 76. Mouat, I.C., Shanina, I. & Horwitz, M.S. Age-associated B cells are long-lasting effectors that
775   impede latent gammaHV68 reactivation. *Sci Rep* **12**, 21189 (2022).
776 77. Elkington, P., Tebruegge, M. & Mansour, S. Tuberculosis: An Infection-Initiated Autoimmune
777   Disease? *Trends Immunol* **37**, 815-818 (2016).
778 78. Belyaeva, I.V., Kosova, A.N. & Vasiliev, A.G. Tuberculosis and Autoimmunity.
779   *Pathophysiology* **29**, 298-318 (2022).
780 79. Joosten, S.A.*, et al.* Mycobacterial growth inhibition is associated with trained innate
781   immunity. *J Clin Invest* **128**, 1837-1851 (2018).
782 80. Singhania, A.*, et al.* A modular transcriptional signature identifies phenotypic heterogeneity
783   of human tuberculosis infection. *Nat Commun* **9**, 2308 (2018).
784 81. Lubbers, R., van Essen, M.F., van Kooten, C. & Trouw, L.A. Production of complement
785   components by cells of the immune system. *Clin Exp Immunol* **188**, 183-194 (2017).
786 82. Weill, J.C. & Reynaud, C.A. IgM memory B cells: specific effectors of innate-like and adaptive
787   responses. *Curr Opin Immunol* **63**, 1-6 (2020).
788 83. Schorey, J.S., Carroll, M.C. & Brown, E.J. A macrophage invasion mechanism of pathogenic
789   mycobacteria. *Science* **277**, 1091-1093 (1997).
790 84. Irvine, E.B.*, et al.* Robust IgM responses following intravenous vaccination with Bacille
791   Calmette-Guerin associate with prevention of Mycobacterium tuberculosis infection in
792   macaques. *Nat Immunol* **22**, 1515-1523 (2021).
793 85. Li, H.*, et al.* Latently and uninfected healthcare workers exposed to TB make protective
794   antibodies against Mycobacterium tuberculosis. *Proc Natl Acad Sci U S A* **114**, 5023-5028
795   (2017).
796 86. Ogongo, P.*, et al.* Differential skewing of donor-unrestricted and gammadelta T cell
797   repertoires in tuberculosis-infected human lungs. *J Clin Invest* **130**, 214-230 (2020).
798 87. Laemmli, U.K. Cleavage of structural proteins during the assembly of the head of
799   bacteriophage T4. *Nature* **227**, 680-685 (1970).
800 88. Andreu, N.*, et al.* Optimisation of bioluminescent reporters for use with mycobacteria. *PLoS
801   One* **5**, e10777 (2010).
802 89. Tezera, L.B., Bielecka, M.K. & Elkington, P.T. Bioelectrospray Methodology for Dissection of
803   the Host-pathogen Interaction in Human Tuberculosis. *Bio Protoc* **7**(2017).
804 90. Reyfman, P.A.*, et al.* Single-Cell Transcriptomic Analysis of Human Lung Provides Insights into
805   the Pathobiology of Pulmonary Fibrosis. *Am J Respir Crit Care Med* **199**, 1517-1536 (2019).

806

807

813 **Author contributions**

814 RK conducted experimental work, data analysis and writing of the manuscript; PO provided initial data,

815 assisted with data analysis and writing; DM assisted with data analysis and writing; LT conducted some

816 biomimetic model experiments, assisted with data analysis and writing; MA, IM, MC, AN, MM assisted

817 in sample preparation; MC assisted with "R" analyses; FK, KK, RM obtained samples and analyzed

818 clinical information; KL, KN assisted with microscopy; A Steyn established the lung cohort; AS assisted

819 with data analysis; PE helped with data interpretation, study design, and manuscript preparation; and

820 AL is the senior author who designed and implemented this study, analyzed the data, and cowrote the

821 manuscript with RK.

822 **Competing interests**

823 The authors declare no competing interests.

824

825

826
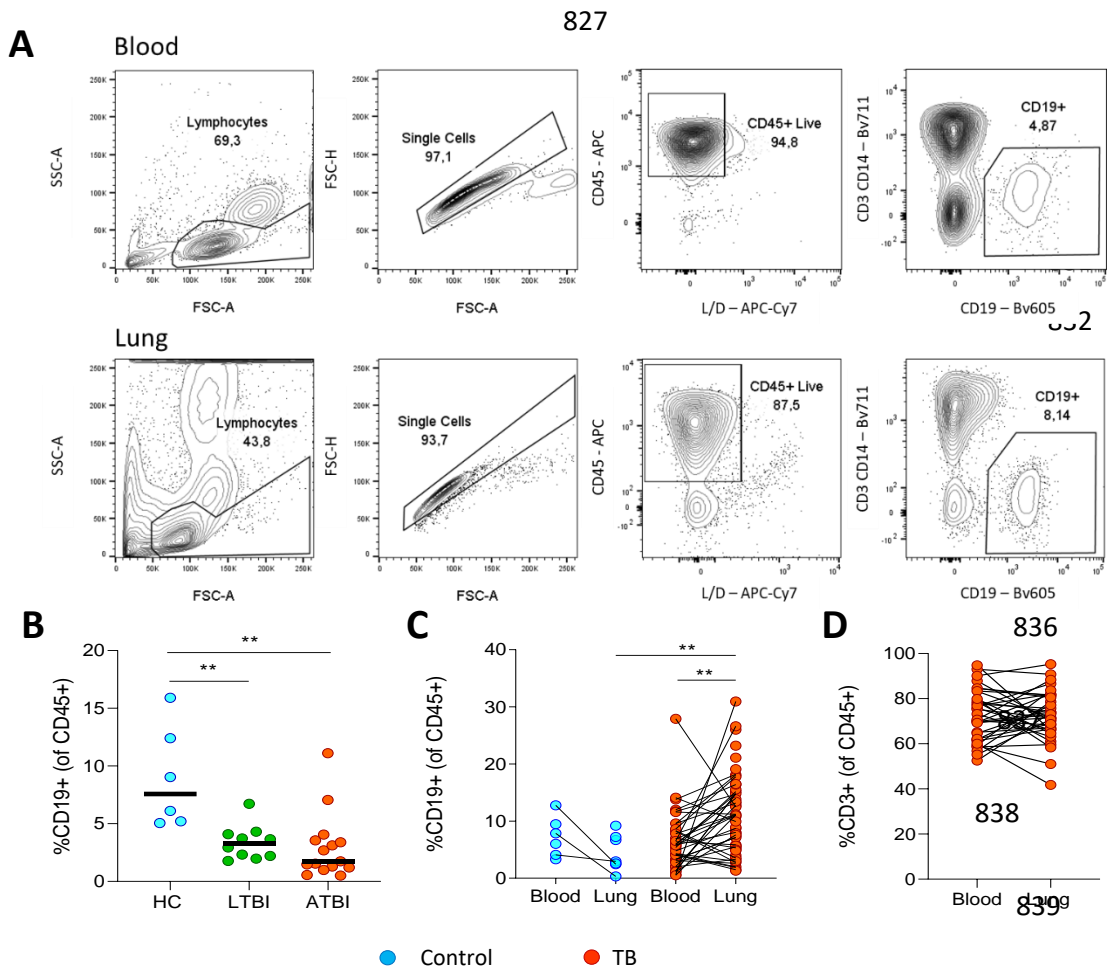
Figure 1: Frequencies of CD19$^+$ B cells differ between blood and lung compartments. (**A**) Representative flow plots identifying CD19$^+$ B cells from peripheral blood monouclear cells (PBMC) and resected lung tissue. (**B**) B cell frequencies in the blood were compared for a set of healthy controls (HC, n=6), latent TB (LTBI, n=10) or active TB (ATBI, n=15) patients, demonstrating reduced circulating B cells in active TB. (**C**) B cell frequencies were compared for lung tissue versus matched blood of cancer control patients (in cyan, n=8) and TB patients (in red, n=60). B cell numbers were increased in the lung compared to the blood in TB patients, and also relative to cancer control lung tissue. (**D**) In contrast, comparative frequencies of CD3$^+$ T cells between lung tissue and matched blood of TB patients showed no significant difference. Statistical analyses were performed using the Mann-Whitney test between unmatched samples and the Wilcoxon test for matched/paired samples. *P* values are denoted by ** < 0.01.
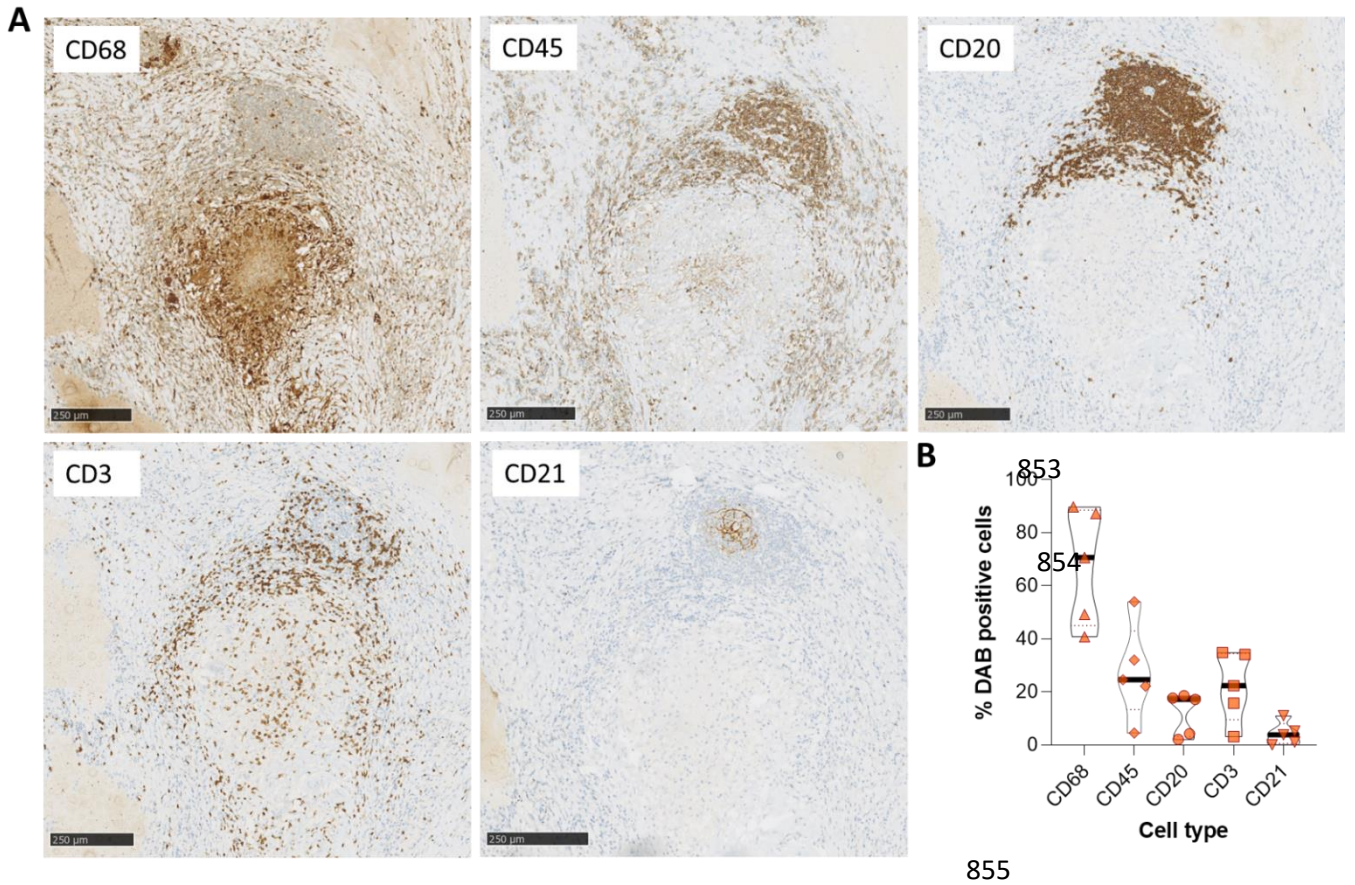
Figure 2: Immunohistochemistry of human lung tissue resection from a TB patient demonstrates B cell aggregates adjacent to the granuloma. (**A**) Serial sections of TB patient lung tissue were stained for macrophages (anti-CD68), leucocytes (anti-CD45), B cells (anti-CD20), T cells (anti-CD3) and dendritic cells (anti-CD21). (**B**) The diaminobenzidine (DAB) stained cells were enumerated and expressed as % DAB positive cells of total nucleated (haematoxylin+) cells, per total slide area imaged. The relative frequencies from a total of five different TB patient tissue samples are compared.

33
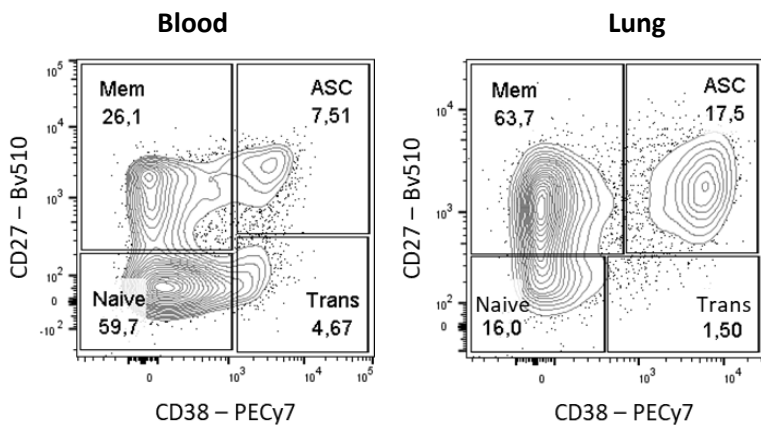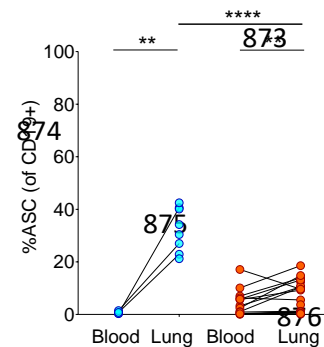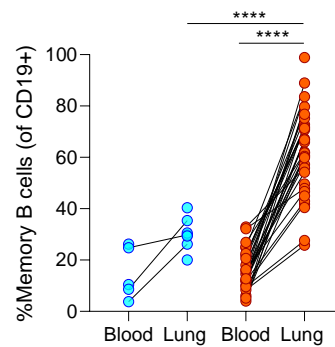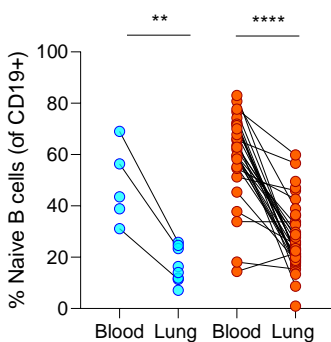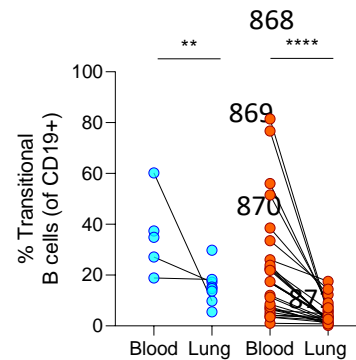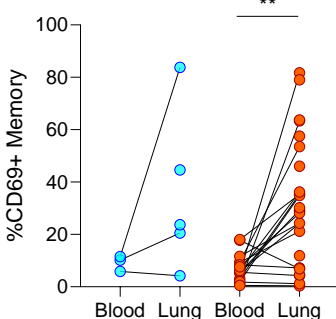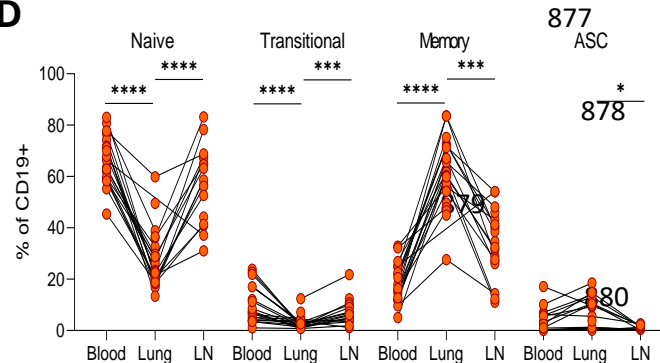
Figure 3: B cell transitional, naïve, memory and antibody secreting cell population frequency demonstrates differences between compartments that are mainly disease-independent. (**A**) Representative flow plots of the canonical transitional (Trans), naïve, memory (Mem) and antibody secreting cell (ASC) B cell phenotypes derived from staining CD19+ B cells with CD27 and CD38 (cancer control in cyan, n=8; TB patients in red, n=60). (**B**) The relative frequencies of these four B cell phenotypes were compared between blood and lung tissue compartments. (**C**) The frequency of CD69$^+$ memory B cells was assessed (cancer control in cyan, n=5; TB patients in red, n=25). (**D**) This analysis was extended to lung draining lymph nodes (LN, n=17) from the TB cohort for comparison. A representative gating strategy for LN derived B cells is included as **Supplementary Figure 2**. Statistical analyses were performed using the Mann-Whitney test between unmatched samples, the Wilcoxon test for matched/paired samples and a three-way Kruskal-Wallis comparison. *P* values are denoted by * ≤ 0.05; ** < 0.01; *** < 0.001 and **** < 0.0001.

894

895

896

897

898

899

900

901

902

903

904

905

906

907

908

909

910

911

912

913

914
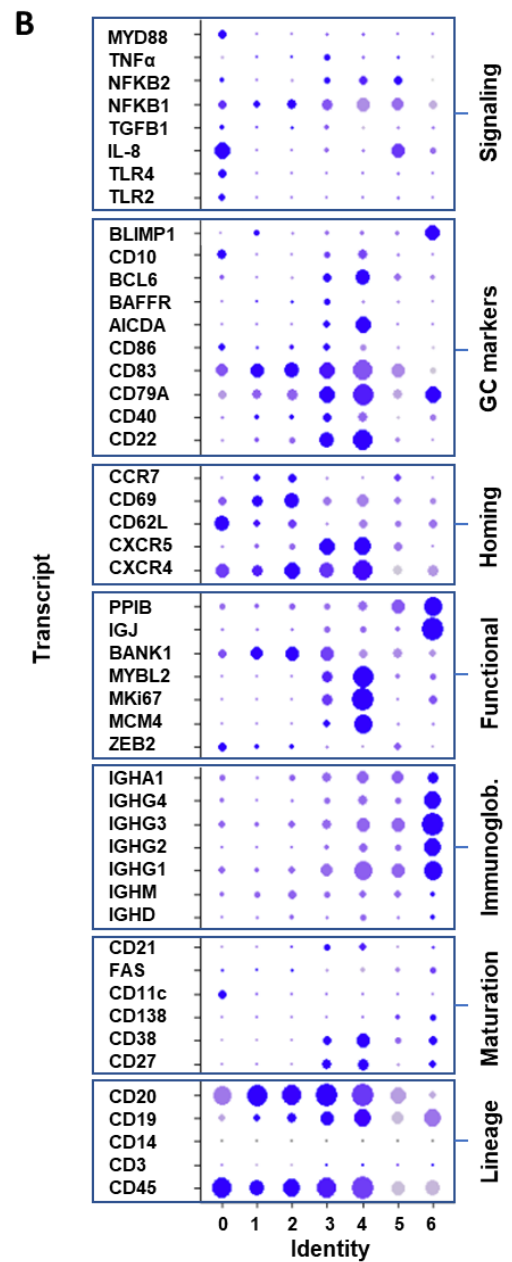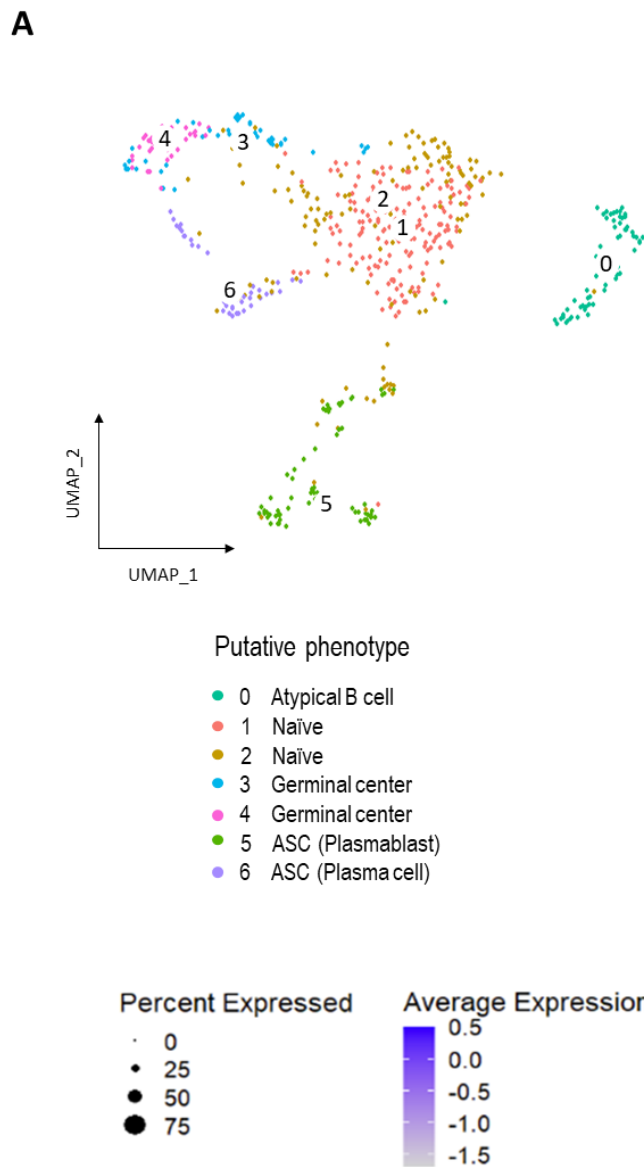
Figure 4: Differential gene expression identifies subclusters amongst B cells isolated from human TB patient lung tissue. scRNA sequencing was used to explore the differentially expressed genes in B cells isolated from human TB patient lung tissue (n=9). (**A**) B cells were clustered based on their differential gene expression and visualised by UMAP with a total of seven putative clusters identified (0 to 6). (**B**) These B cell clusters were interogated for their expression of specific B cell-associated genes to delineate their likely functions.

921

922

923
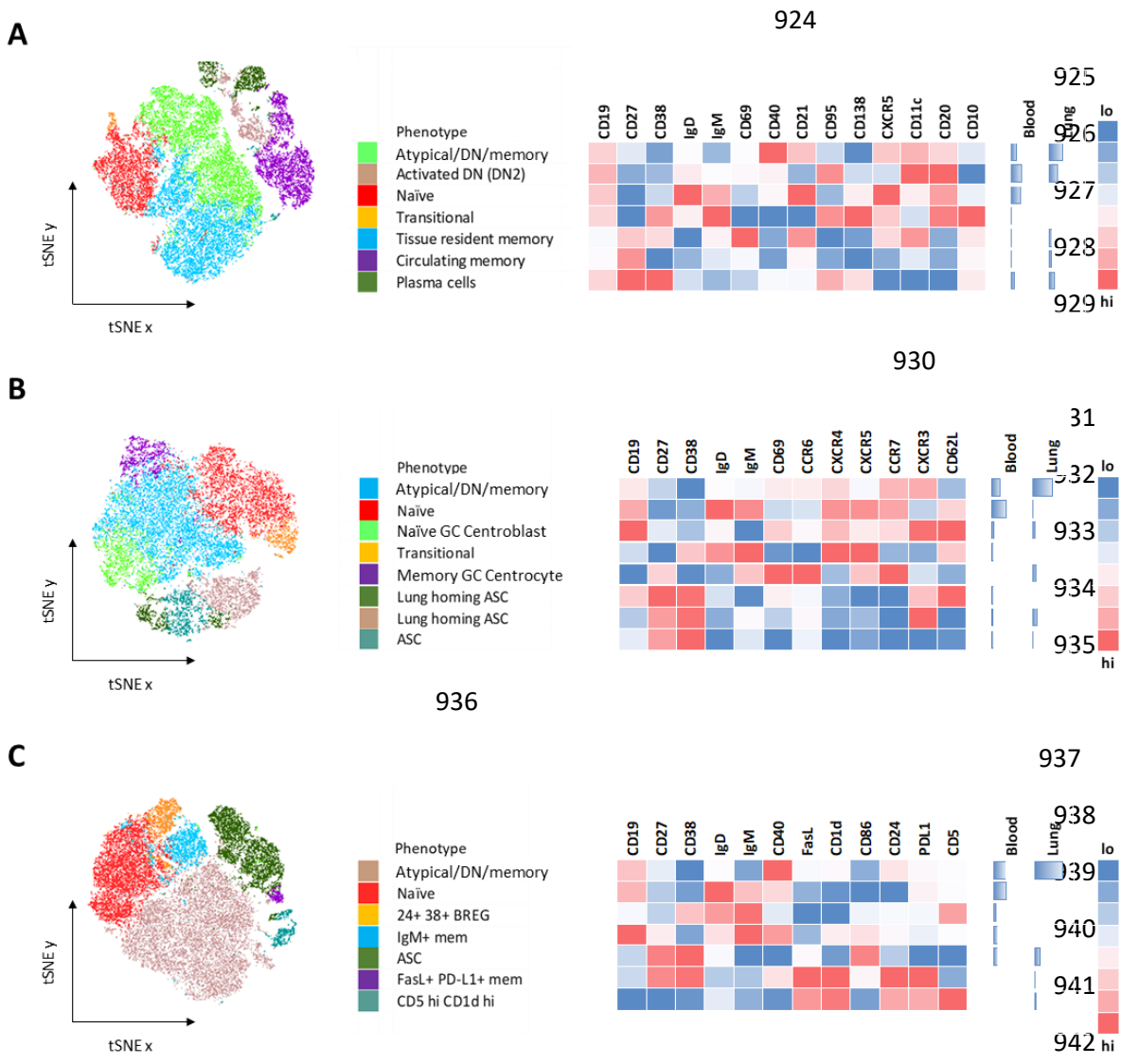
Figure 5: tSNE plot comparison of B cell phenotypes further refines blood and lung tissue associated compartments. In order to study the complexity of the B cell phenotypes associated with TB patient blood and lung tissue compartments, three separate flow cytometry phenotyping panels were used. (**A**) Assesed the level of maturation of the B cells, (**B**) the expression of different homing markers and (**C**) the relative expression of regulatory markers. The different B cell populations were clustered spatially using tSNE, with a single patient presented here, followed by a key describing the major phenotypes each of which is assigned a different colour. The relative expression of the specific markers associated with each phenotype were plotted alongside in a heatmap. Since the blood and lung samples were concatenated into a single file, the relative frequencies of cells in the blood or lung tissue compartment could be compared as shown alongside the heatmap.

957
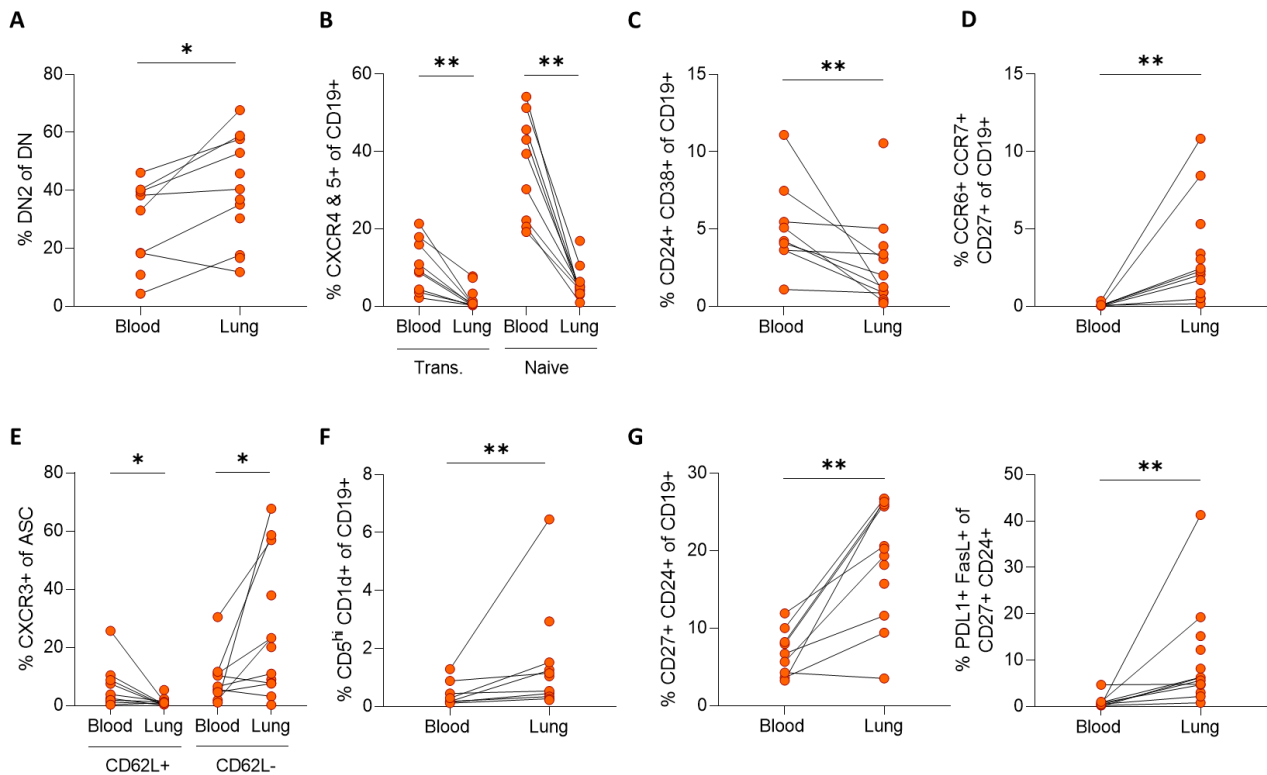
Figure 6: tSNE-derived unique B cell phenotypes associated with the blood or lung compartment of TB patients. (**A**) Double negative (DN) B cells (CD27⁻IgD⁻) were assessed and the activated (DN2) pehnotype (CD21⁻CD11c⁺) was enriched in TB patient lungs. (**B**) GC homing (CXCR4⁺CXCR5⁺) transitional and naïve B cells were enriched in the blood compartment. (**C**) The blood compartment was enriched for a tranistional regulatory (CD24⁺CD38⁺) population. (**D**) The lung compartment contained a unique activated B cell memory (CD27⁺CXCR5⁺CD62L⁻CD69⁺CCR6⁺CCR7⁺) population. (**E**) Lung derived ASC populations expressed a CXCR3⁺CD62L⁻ phenotype relative to the blood derived counterparts. Other B cell phenotypes associated with regulatory functions were enriched in the lung, including (**F**) a CD5⁺ phenotype (CD5ʰⁱCD40⁻CD1d⁺) and (**G**) a CD27⁺ regulatory population (CD27⁺CD24⁺FasL⁺PDL1⁺). A set of 13 TB patient samples were used in these analyses. Statistical analyses were performed using the Wilcoxon test for matched/paired samples. *P* values are denoted by * ≤ 0.05 and ** < 0.01.

958
959
960
961
962
963
964
965
966
967
968
969

970
971
972
973
974
975
976
977
978
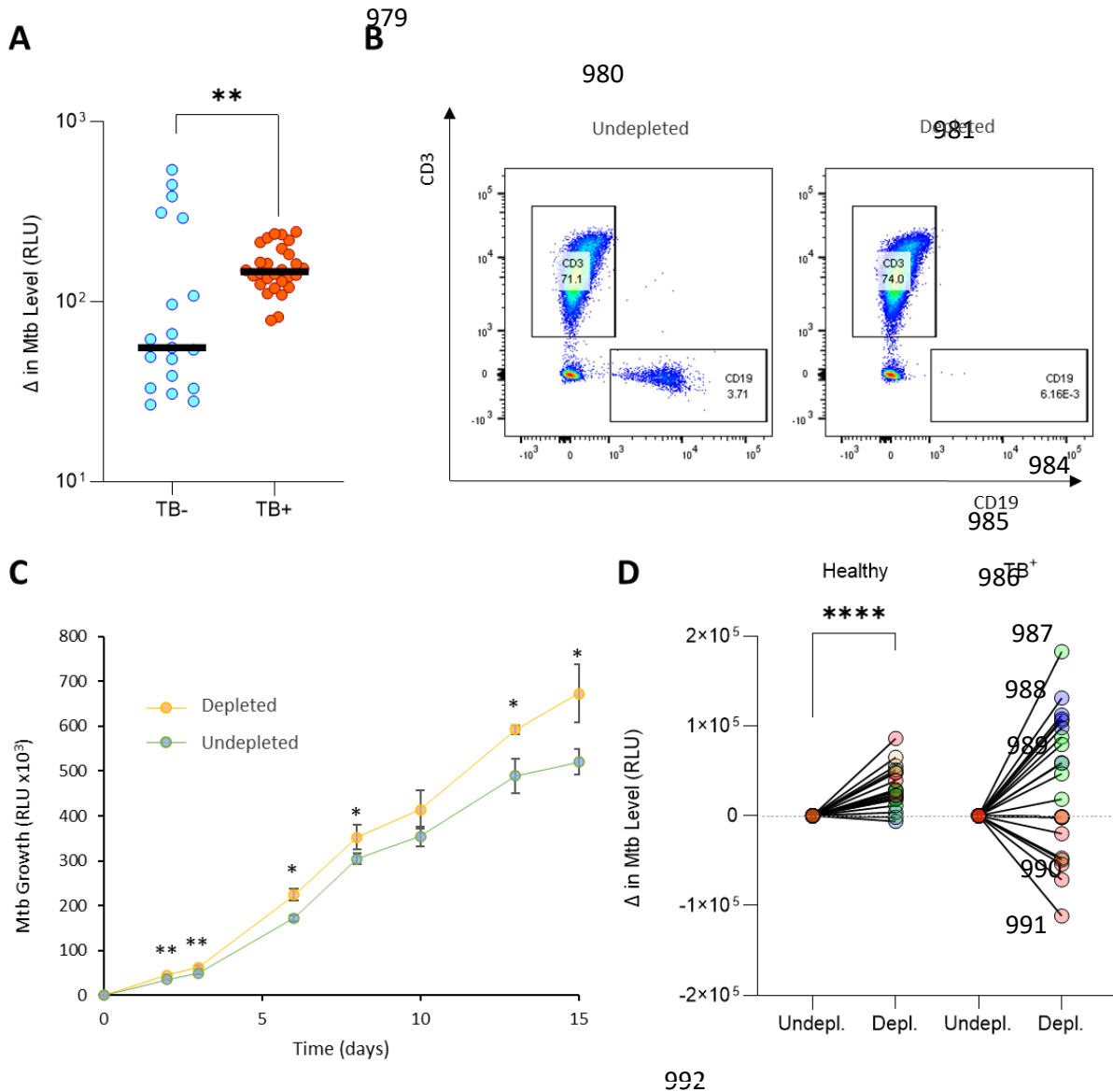
Figure 7: B cells contribute to host control of *Mtb* in healthy donors in a 3D biomimetic model, but in TB patients the effect is highly variable. (A) Comparatively, *Mtb* grew more rapidly in TB patient derived PBMC. B cells were depleted from PBMCs, of which four donors were healthy and four had active TB, and compared to undepleted PBMCs. (**B**) Representative FACS plots of the depletion process. (**C**) B cell depletion leads to significantly higher *Mtb* growth in a healthy donor PBMC sample, representative of four healthy donors. (**D**) *Mtb* outgrowth data at day 7 from a total of four PBMC donors from each group are summarized, demonstrating the highly variable effect of B cell depletion in TB patients. Data were normalized to the undepleted control group and compared by Wilcoxon matched-pairs signed rank test. *P* values are denoted by * ≤ 0.05; ** < 0.01 and **** < 0.0001.
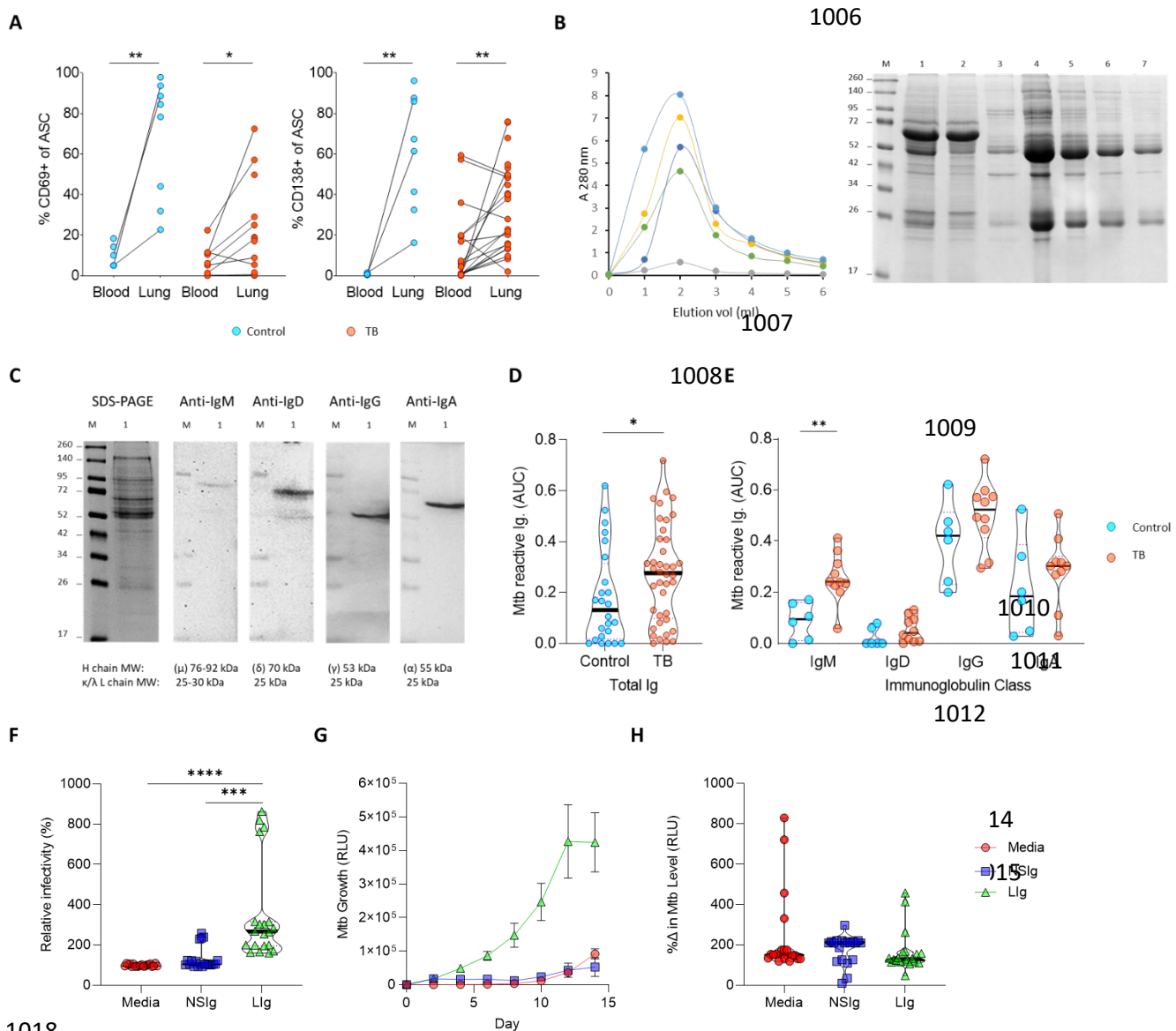
Figure 8: Mature CD138+ plasma cells are enriched in the lung tissue, resulting in an upregulated *Mtb* specific antibody response that enhances *Mtb* phagocytosis. (**A**) The tissue residence marker CD69 was expressed on antibody secreting cells (ASC), with the majority displaying a mature plasma cell CD138+ phenotype in both cancer controls (n=8) and TB patients (n=13 to 25). (**B**) Antibodies were isolated from homogenised lung tissue supernatants using a thiophilic resin, with example elution profiles from five lungs measured at 280 nm, and then examined on a reducing 12.5% SDS-PAGE gel. The molecular weight marker (lane M), was followed by the initial lung homogenate supernatant sample (lane 1), the unbound sample (lane 2) followed by the eluted fractions 1-5 from the elution profile alongside (lanes 3-7). (**C**) Peak eluents (lane 1) were tested for the presence of IgM, IgD, IgG and IgA using class-specific secondary antibodies by Western blot. (**D**) *Mtb* specific antibody binding was investigated in samples from cancer control (n=6) and TB patient lungs (n=10), detecting both total reactivity and (**E**) class-specific responses in a direct ELISA based approach, expressed as area under the curve (AUC). An equal concentration range (100 to 0.8 µg/ml) of isolated antibody was used to standardize the assay and allow for comparison between patients. Antibody frequencies were compared by Mann-Whitney test. (**F**) *Mtb* phagocytosis by PBMCs was compared between untreated

Mtb versus *Mtb* treated with non-specific immunoglobulin (NSIg) or TB lung immunoglobulin (LIg). The lung-derived immunoglobulin increased phagocytosis, whilst non-specific immunoglobulin had no effect. Data are presented as summary data from five TB patient immunoglobulin samples tested with three different PBMC donors, with each experiment done in quadruplicate and infectivity was measured by luminescence. Data were normalized to the media control and the donor matched mean differences were compared by one way ANOVA. (**G**) Representative *Mtb* growth using TB patient immunoglobulin comparing with untreated and non-specific immunoglobulin in the 3D biomimetic model of TB. (**H**) *Mtb* luminescence at day 8 normalized to day 0 initial infectious load shows no overall difference in growth rate over time. *P* values are denoted by * ≤ 0.05; ** < 0.01; *** < 0.001 and **** < 0.0001.

Supplementary information
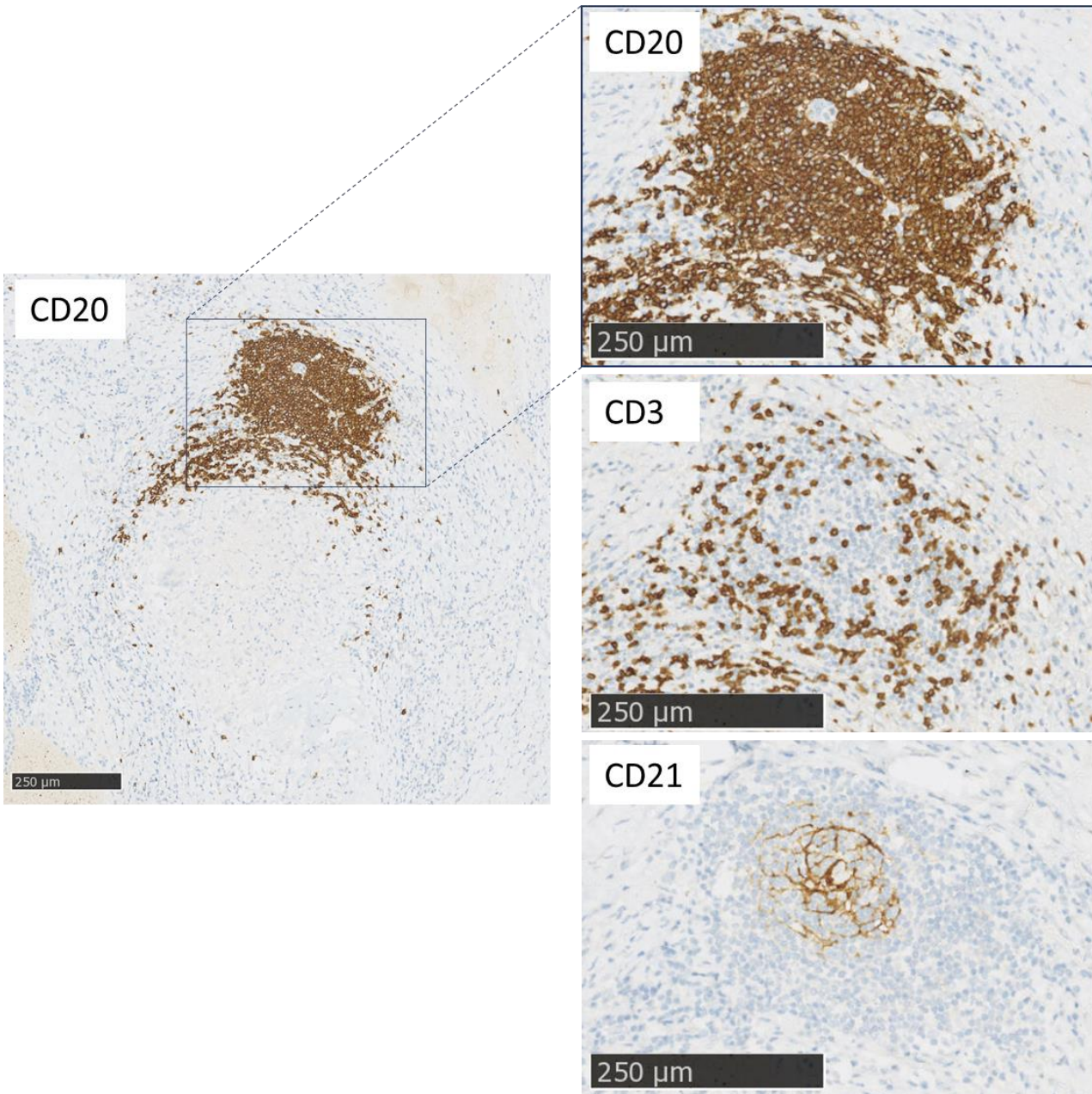
Supplementary Figure 1: Immunohistochemistry of human lung tissue resection from a TB patient
demonstrates cellular organisation within aggregates associated with the granuloma. Serial
sections of TB patient lung tissue were stained for B cells (anti-CD20), T cells (anti-CD3) and dendritic
cells/mature B cells (anti-CD21). The boxed region is enlarged to illustrate the distinct staining
patterns of the different markers within the granuloma associated aggregates.
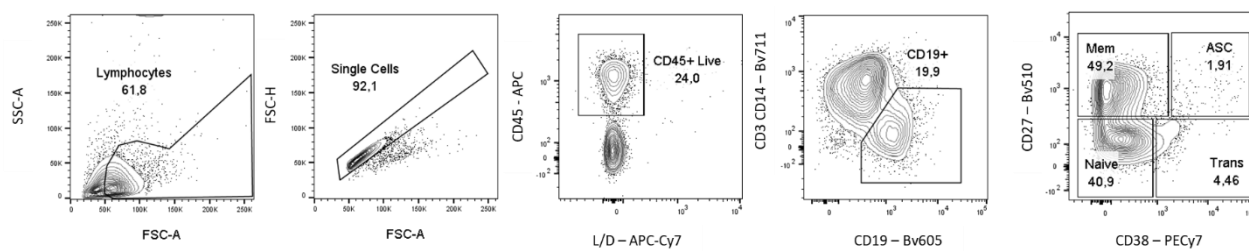
1087 **Supplementary Figure 2: Gating strategy to identify CD19$^+$ B cells associated with the lung draining**
1088 **lymph node.** Representative flow plots identifying CD19$^+$ B cells derived from the lung draining lymph
1089 node of TB patient lungs. This was followed by gating the canonical transitional, naïve, memory and
1090 ASC phenotypes derived from staining the B cells with CD27 and CD38.
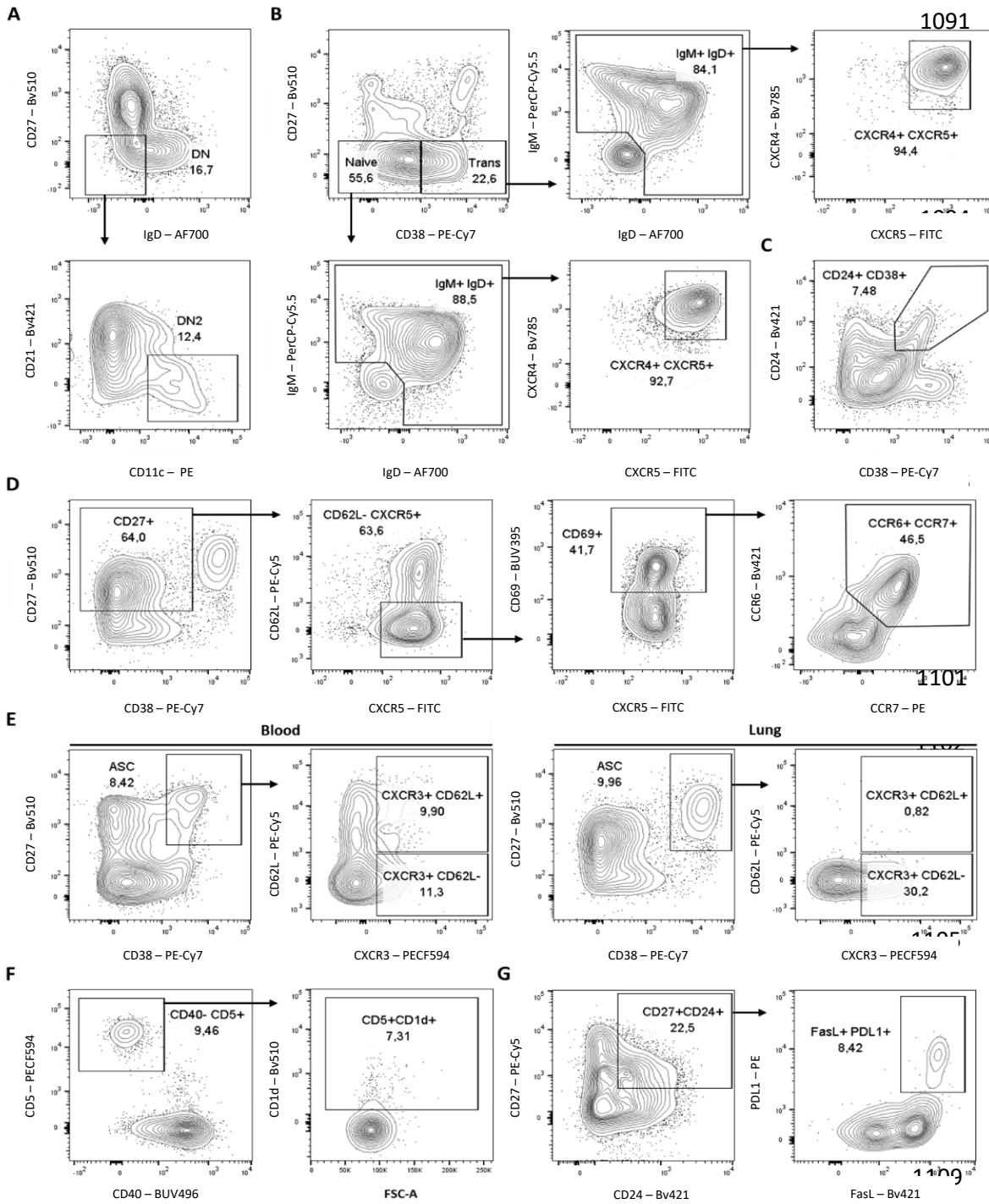
1110

Supplementary Figure 3: Gating strategies for t-SNE derived B cell phenotypes associated with the blood or lung compartment. (**A**) Double negative (DN, CD27- IgD-) and activated DN (CD21- CD11c+) B cells. (**B**) Blood derived GC homing (CXCR4+ CXCR5+) transitional and naïve B cells. (**C**) Blood enriched tranistional regulatory (CD24+ CD38+) B cells. (**D**) The lung derived activated B cell memory (CD27+ CXCR5+ CD62L- CD69+ CCR6+ CCR7+) population. (**E**) Respective Blood and Lung derived ASC populations expressing a CXCR3 and/or CD62L. (**F**) A lung enriched CD5+ phenotype (CD5^{hi} CD40- CD1d+) and (**G**) a CD27+ regulatory population (CD27+ CD24+ FasL+ PDL1+).
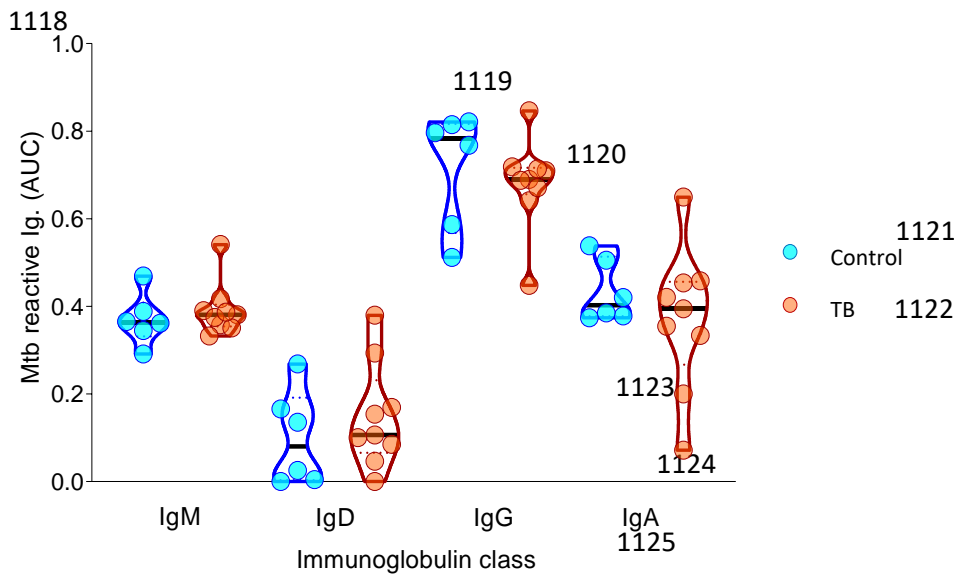
1126

Supplementary Figure 4: *Mtb* **specific response in patient plasma derived antibodies by ELISA.** The *Mtb* specific antibody responses from cancer control (n=6) and TB patient (n=9) plasma, detecting class-specific responses. There were no significant differences as compared by Mann-Whitney test.